Final Report *December 1985*

INFRARED PROPERTIES OF BIOLOGICAL MATERIALS OF INTEREST TO THE ARMY

By: D. E. COOPER D. D. POWELL

Prepared for:

U.S. ARMY RESEARCH OFFICE
P. O. BOX 12211
RESEARCH TRIANGLE PARK, NORTH CAROLINA 27709

CONTRACT DAAG29-82-K-0126

SRI Project 4504

SRI International
333 Ravenswood Avenue
Menlo Park, California 94025
(415) 326-6200
Cable: SRI INTL MPK
TWX: 910-373-2046

SRI International®

The views, opinions, and/or findings contained in this report are those of the author(s) and should not be construed as an official Department of the Army position, policy, or decision, unless so designated by other documentation.

SRI International

Final Report *December 1985*

INFRARED PROPERTIES OF BIOLOGICAL MATERIALS OF INTEREST TO THE ARMY

By: D. E. COOPER D. D. POWELL

Prepared for:

U.S. ARMY RESEARCH OFFICE
P. O. BOX 12211
RESEARCH TRIANGLE PARK, NORTH CAROLINA 27709

CONTRACT DAAG29-82-K-0126

SRI Project 4504

Approved for public release, distribution unlimited.

Approved by:

EDWARD R. MURRAY, *Director*
Electro-Optics Systems Laboratory

LAWRENCE E. SWEENEY, JR., *Executive Director*
System Technology Division

SRI INTERNATIONAL, 333 Ravenswood Avenue, Menlo Park, California 94025
(415) 326-6200, Cable: SRI INTL MPK, TWX: 910-373-2046

SRI International (R)

UNCLASSIFIED

SECURITY CLASSIFICATION OF THIS PAGE

AD-A164 351

REPORT DOCUMENTATION PAGE

1a. REPORT SECURITY CLASSIFICATION UNCLASSIFIED	1b. RESTRICTIVE MARKINGS
2a. SECURITY CLASSIFICATION AUTHORITY n/a	3. DISTRIBUTION/AVAILABILITY OF REPORT Approved for public release; distribution unlimited
2b. DECLASSIFICATION/DOWNGRADING SCHEDULE n/a	
4. PERFORMING ORGANIZATION REPORT NUMBER(S) SRI Project 4504 Final Report	5. MONITORING ORGANIZATION REPORT NUMBER(S) ARO 17889.2-CS
6a. NAME OF PERFORMING ORGANIZATION SRI International 6b. OFFICE SYMBOL (If applicable)	7a. NAME OF MONITORING ORGANIZATION
6c. ADDRESS (City, State, and ZIP Code) 333 Ravenswood Avenue Menlo Park, California 94025	7b. ADDRESS (City, State, and ZIP Code)
8a. NAME OF FUNDING/SPONSORING ORGANIZATION U.S. Army Research Office 8b. OFFICE SYMBOL (If applicable)	9. PROCUREMENT INSTRUMENT IDENTIFICATION NUMBER
8c. ADDRESS (City, State, and ZIP Code) P.O. Box 12211 Research Triangle Park, North Carolina 27709	10. SOURCE OF FUNDING NUMBERS PROGRAM ELEMENT NO. / PROJECT NO. / TASK NO. / WORK UNIT ACCESSION NO.

11. TITLE (Include Security Classification)

Infrared Properties of Biological Materials of Interest to the Army

12. PERSONAL AUTHOR(S)
D. E. Cooper, D. D. Powell

13a. TYPE OF REPORT	13b. TIME COVERED	14. DATE OF REPORT (Year, Month, Day)	15. PAGE COUNT
Final	FROM 5/82 TO 12/85	December 1985	

16. SUPPLEMENTARY NOTATION

17. COSATI CODES			18. SUBJECT TERMS (Continue on reverse if necessary and identify by block number)
FIELD	GROUP	SUB-GROUP	biological organisms; aerosols; infrared properties; differential scattering (DISC); circular-intensity differential scattering (CIDS)

19. ABSTRACT (Continue on reverse if necessary and identify by block number)

The infrared (IR) properties of lyophilized E. coli, B. subtilis, B. subtilis spores, and M. luteus were measured to determine the utility of IR differential scatter (DISC) for remote detection of biological aerosol clouds. Specifically, the complex refractive indices of these materials were measured in the 4000- to 180-cm^{-1} (2.5- to 40-μm) spectral region. IR backscatter was measured from aerosols of these materials over the 9- to 11-μm region using a tunable CO_2 laser. The observed backscatter signatures were found to be in agreement with the predictions of Mie theory, which uses as input the measured complex refractive indices of the specific materials. Based on this work, we concluded that IR DISC is capable of detecting aerosols of biological organisms only at concentrations exceeding 10^5 particles/liter, which does not meet the Army's stated sensitivity requirement of 5 to 20 particles/liter. This sensitivity limitation is due to the relatively featureless 9- to 11-μm IR spectra of microorganisms and to the differential scattering of the natural atmospheric aerosol background.

20. DISTRIBUTION/AVAILABILITY OF ABSTRACT	21. ABSTRACT SECURITY CLASSIFICATION
☐ UNCLASSIFIED/UNLIMITED ☒ SAME AS RPT. ☐ DTIC USERS	UNCLASSIFIED
22a. NAME OF RESPONSIBLE INDIVIDUAL	22b. TELEPHONE (Include Area Code) / 22c. OFFICE SYMBOL

DD FORM 1473, 84 MAR

83 APR edition may be used until exhausted. All other editions are obsolete.

SECURITY CLASSIFICATION OF THIS PAGE

UNCLASSIFIED

18. SUBJECT TERMS (continued)

refractive index	E. Coli	T2 virus
extinction	B. Subtilis	T4 virus
remote detection	M. Luteus	

19. ABSTRACT (continued)

In an attempt to overcome the sensitivity limitations of DISC, we considered polarization-sensitive detection techniques in the final year of the contract. The technique chosen for further study was circular-intensity differential scattering (CIDS), or differential scattering of circularly polarized light caused by the chiral structures of biological macromolecules. We measured CIDS from liquid suspensions of T2 and T4 viruses and from the bacteria E. Coli. The measurements were made at fixed scattering angles of 90° and 168° over the 350- to 600-nm spectral region. Typical CIDS signals were in the range of 10^{-4} to 10^{-3}. The near-backscatter (168°) CIDS signals were in all cases about one order of magnitude smaller than the 90° signals. The CIDS spectra from these materials did not exhibit distinctive features that might be used for local or in-situ aerosol detection using a lidar-type backscatter system. We concluded that CIDS will probably only prove viable as a detection technique in circumstances where measurements can be made on a liquid suspension at different angles and at different wavelengths. In addition, it will likely prove necessary to measure simultaneously several Mueller scattering matrix elements to obtain a unique signature for detection of biological microorganisms. CIDS as a point detector shows promise of meeting the array's sensitivity goal.

CONTENTS

LIST OF ILLUSTRATIONS

ILLUSTRATONS (Continued)

I INTRODUCTION

A U.S. capability for remote and point detection of biological agents has become a rapidly expanding need in view of past and present Soviet activities. Remote sensing is particularly important because early warning of the presence of these agents can provide critical time needed for complete and effective protection.

The purpose of this research was to establish the fundamental interaction between infrared (IR) radiation and biological materials so that the feasibility of using active and passive IR techniques for remote detection and alarm can be evaluated. Data concerning IR properties of biological materials may also be helpful in the development of techniques for identification of biological species.

The objectives of this work were to:

- Measure the index of refraction of several biological materials in the wavelength region of 2 to 14 μm.
- Establish a data base of measured backscatter and extinction signatures as functions of wavelength for selected biological materials in the aerosol state.
- Compare measured backscatter and extinction signatures with values calculated using standard spherical and nonspherical particle theories to test the accuracy of these theories in calculating the IR properties of biological materials.
- Investigate the ability to discriminate biological particles normally present in the atmosphere by observation and suitable processing of scattering and extinction data.

We first investigated the IR differential scatter (DISC) technique for remote sensing of biological aerosols. The DISC technique relies on the fact that aerosol backscatter spectra show features related to the wavelength dependence of the index of refraction.[1] The index of refraction, in turn, depends on the composition of the aerosol. Thus, a measurement of the backscattering spectrum can yield information about

aerosol composition. IR backscattering signatures from aerosols with a specified size distribution are also uniquely related to composition. However, based on our results, we concluded that IR DISC does not meet the U.S. Army's biological aerosol particle detection sensitivity goal of 5 to 10 particles/liter.

We then investigated circular-intensity differential scattering (CIDS)[2] for remote sensing of biological microorganisms. CIDS is essentially the differential scattering of light from biological aerosols that is left and right circularly polarized due to the chiral structure of biological macromolecules. The CIDS technique showed promise of meeting the Army's sensitivity goal.

II SUMMARY OF IMPORTANT RESULTS

A. Infrared Differential Scattering (IR DISC)

During the first two years of this project, we investigated the IR DISC technique and performed the following work:

(1) Measured complex refractive indices of five biological materials.

(2) Measured backscatter in the 9- to 11-μm region for three biological materials in different concentrations and compared the measured backscatter with theoretical calculations of expected values based on the measured complex refractive indices.

(3) Performed sensitivity calculations based on the measured backscatter to evaluate the use of IR DISC for remote sensing of biological aerosols.

The results of each task are presented below.

1. Complex Refractive Indices

Professor Marvin Querry of the University of Missouri measured complex refractive indices for: (1) lyophilized E. coli, (2) lyophilized M. luteus, (3) lyophilized B. subtilis, (4) lyophilized B. subtilis spores, and (5) aerosolized E. coli. As a first step, near-normal incidence reflectance spectra were obtained for the materials. For lyophilized E. coli and aerosolized E. coli, initial values of the refractive indices were obtained by Kramers-Kronig (KK) analysis of the reflectance data. The values for the refractive indices in the 9- to 11-μm region are compared in Figure 1 for the aerosolized and lyophilized E. coli samples. Although the magnitudes of the refractive indices differ slightly, their variations with wavelength are nearly identical. Since the observed differences are within normal experimental uncertainty in the measured reflectance spectra, we do not consider them significant.

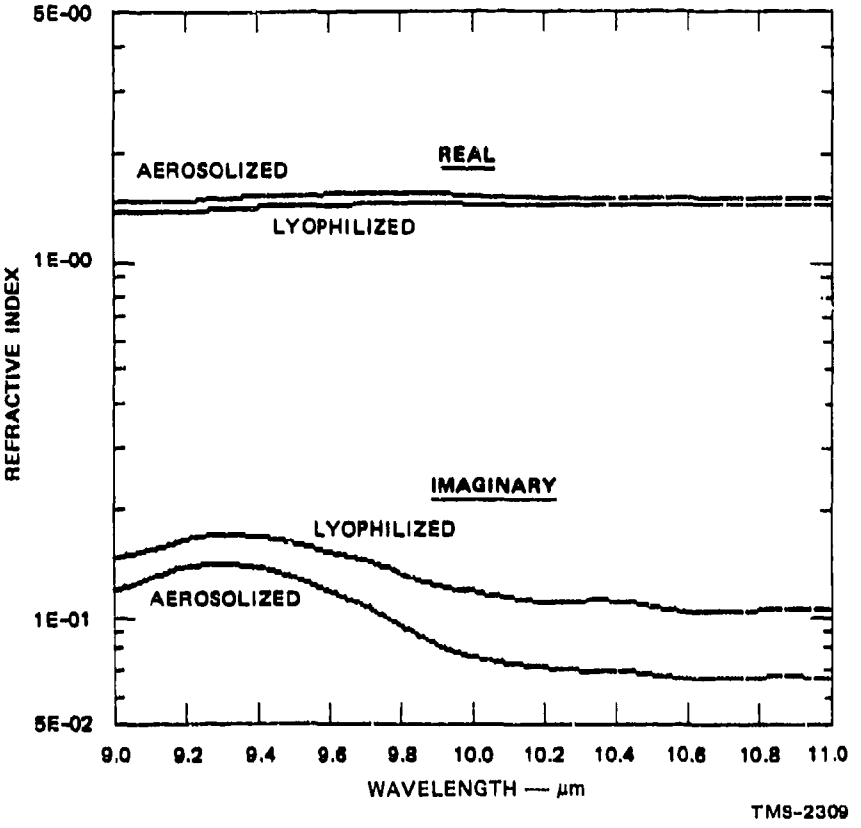

FIGURE 1 COMPARISON OF COMPLEX INDICES OF REFRACTION OF AEROSOLIZED AND LYOPHILIZED *E. COLI*

We therefore performed all remaining refractive index measurements on lyophilized preparations because they are less expensive to prepare.

Complex refractive indices based on the combined use of reflectance and transmittance spectra are generally superior to those obtained with reflectance spectra only. Therefore, once the reflectance spectra were measured, initial values of the complex refractive indices, $N = n + ik$, for each material were obtained by applying the KK methods to the reflectance spectra. Then transmittance spectra were acquired. The relative k spectra (the imaginary part of the refractive index) obtained from the transmittance spectra were then calibrated using the k values

of selected band centers obtained from the KK analysis. Values of the real part of the refractive index, n, were then determined by substituting the calibrated k spectra from the transmittance spectra and the measured reflectance spectra into the appropriate Fresnel reflectance equation.

The reflectivities and real and imaginary parts of the complex refractive index spectra for lyophilized and aerosolized E. coli, lyophilized B. subtilis, B. subtilis spores, and lyophilized M. luteus are compared in Figure 2 for the 9- to 11-μm region. Although all the organisms exhibit qualitatively the same refractive index spectra, there is a distinct difference between the spectra of B. subtilis and B. subtilis spores. These differences are most pronounced for the imaginary component of the refractive index and are expected because of differences in the cell-wall constituents of B. subtilis and B. subtilis spores.

2. IR Backscatter from Biological Aerosols and Comparison with Theory

a. System Description

For this study, we constructed a biological aerosol generator and chamber and breadboarded the necessary optical components and laser for the backscattering measurements in the 9- to 11-μm region. Figure 3 shows the biological aerosol apparatus. The aerosol generator is the slender plexiglass column at right. The larger plexiglass structure on the left is the chamber in which the aerosol clouds were dispersed for the optical measurements. To generate a biological aerosol, a solution of microorganisms is dispersed from syringes at a predetermined flow rate to the aerosol generator. The solution is combined with a stream of heated air which evaporates the water, creating a dry aerosol column in the generator. The column flows through the optical chamber and is contained by air curtains.

IR backscattering spectra from the aerosols were measured in the 9- to 11-μm region using a CO_2 waveguide laser. A schematic diagram of the

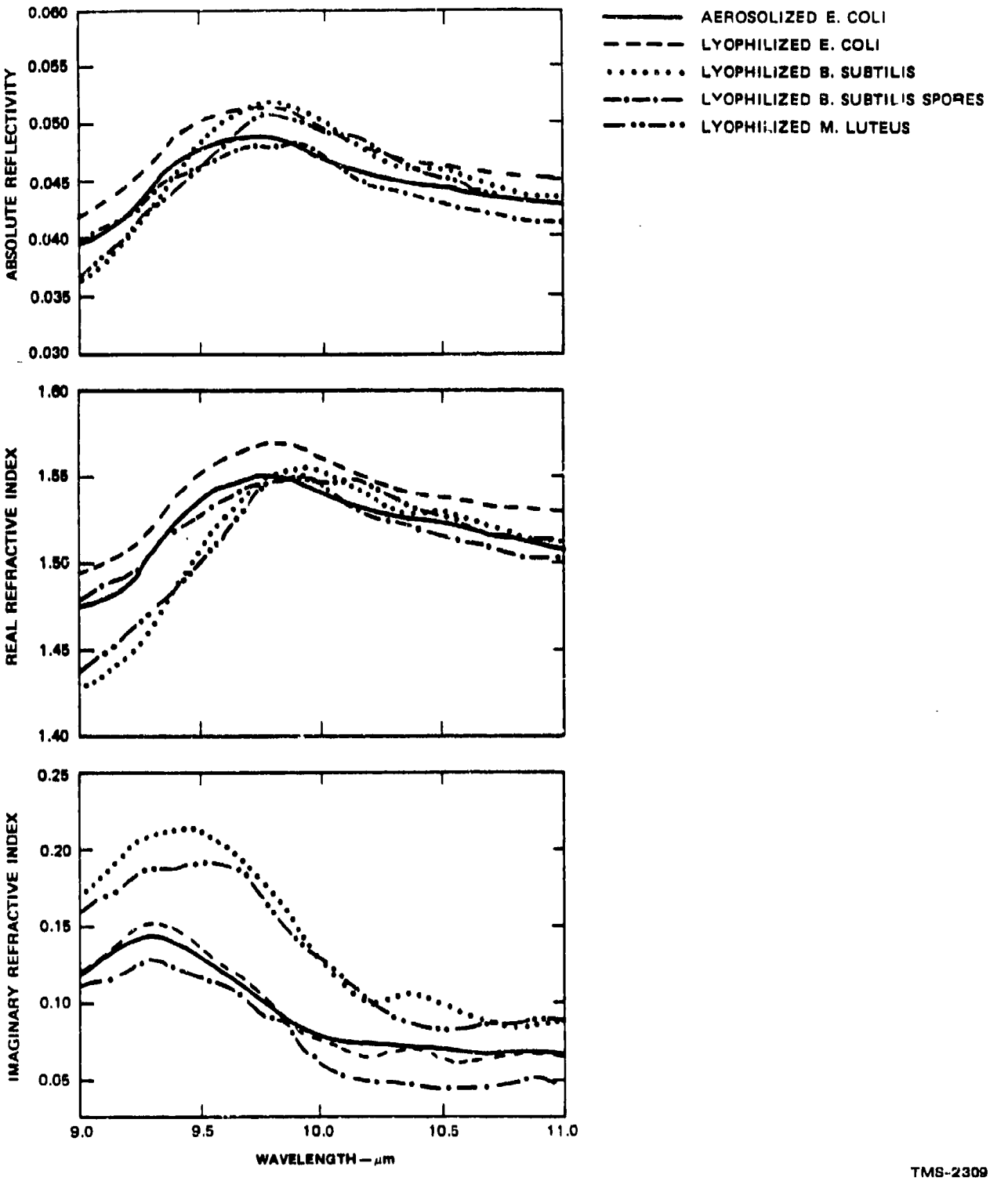

FIGURE 2 REFLECTIVITY AND COMPLEX REFRACTIVE INDICES IN THE 9- TO 11-μm REGION FOR 5 BIOLOGICAL MATERIALS

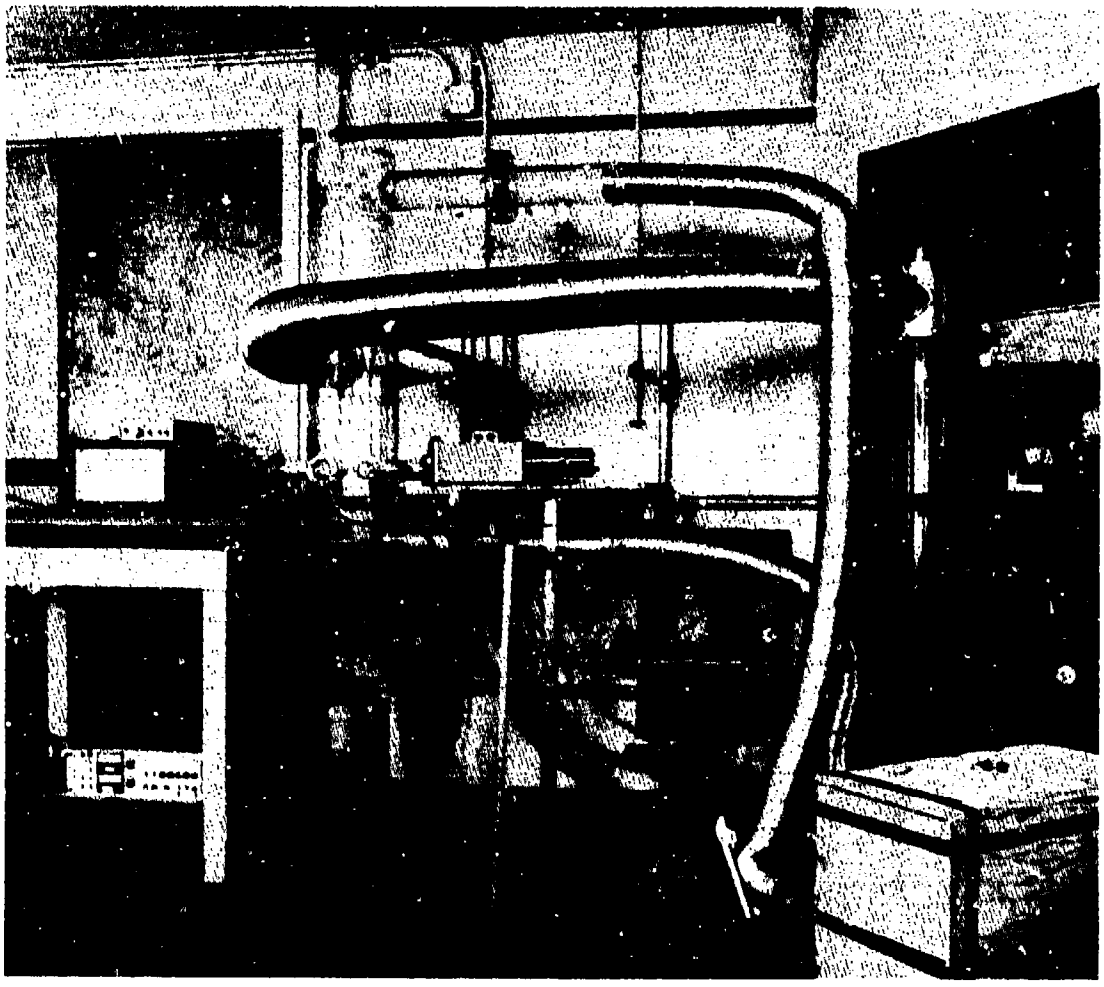

TMS-2309

FIGURE 3 SRI BIOLOGICAL AEROSOL GENERATOR AND CHAMBER

optical system and aerosol generator is shown in Figure 4. The continuous wave (CW) laser beam is chopped at 100 Hz. The chopper also serves as a beamsplitter to divert part of the beam to a pyroelectric power monitor. The chopped laser signal is directed up through the aerosol column. Energy backscattered from the column is collected by a 7.7-cm diameter off-axis parabolic mirror and focused onto a HgCdTe detector. The detector signal is amplified and filtered by a lock-in

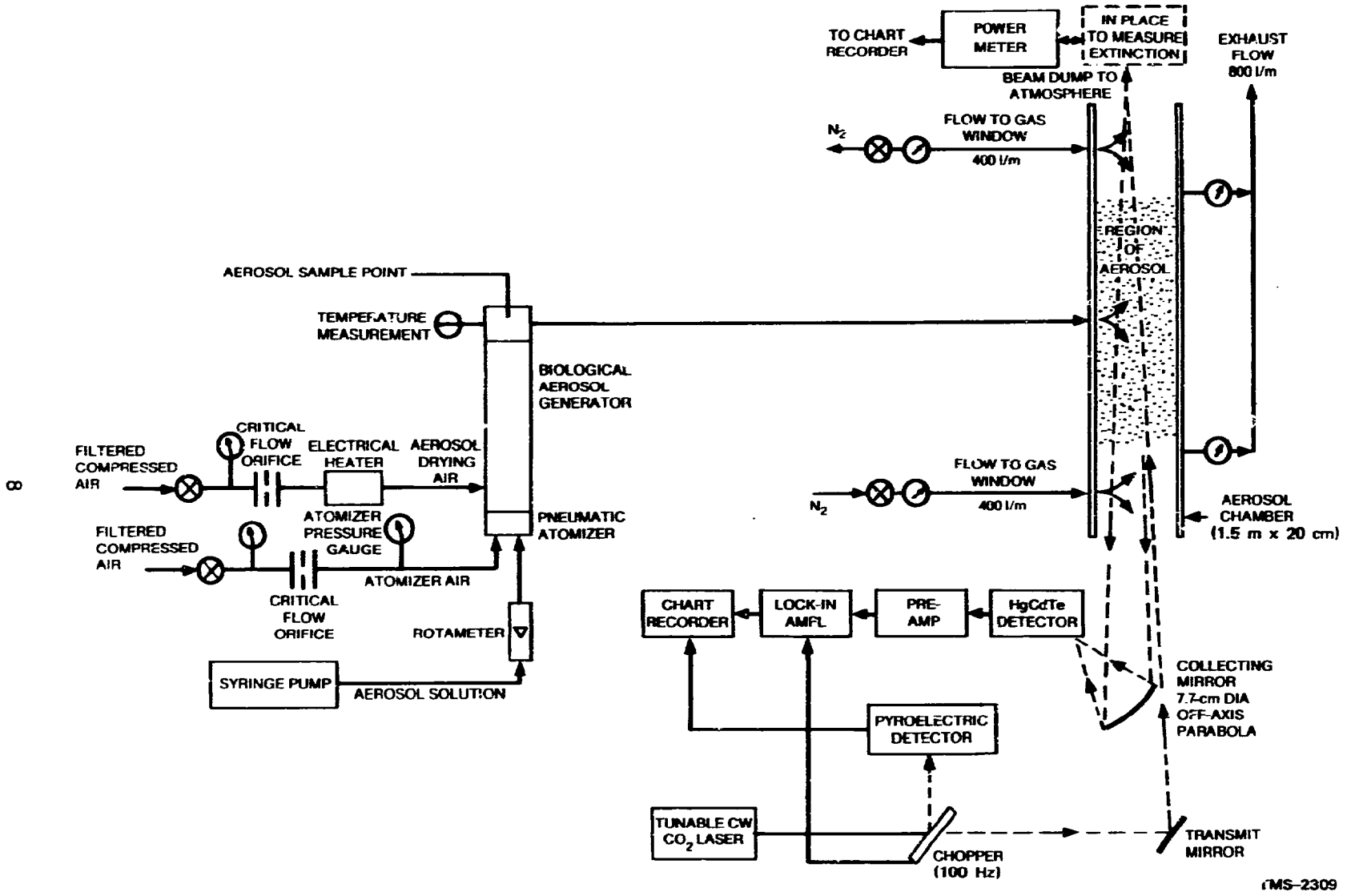

FIGURE 4 AEROSOL GENERATOR AND EQUIPMENT FOR MEASUREMENT OF 9- TO 11-μm BACKSCATTER AND EXTINCTION FROM BIOLOGICAL DISPERSIONS

amplifier referenced to the chopping frequency. The lock-in output is recorded with the laser power on a dual channel chart recorder.

To calibrate the optical system responsivity as a function of wavelength, our first backscattering measurements were performed on aerosols of KBr. This material was chosen because its complex refractive index in the 9- to 11-μm region is well known and essentially flat. It is also soluble in water, so it can be dispersed by the same methods as the biological aerosols. Finally, it was empirically found to form aerosols consisting predominantly of spherical particles, which allowed for a comparison of experimental data with Mie theory predictions.

We generated a KBr aerosol cloud using a 1% concentration solution in the syringe pump. A particle cascade impactor was used to measure the aerosol size distribution at the center of the chamber. The size distribution was found to be log-normal with a mass-median diameter (MMD) of 0 9 μm and a geometric standard deviation of 2.49.

Using these parameters and the KBr refractive indices, we calculated with a Mie code the expected backscattering signature over the CO_2 laser wavelength region. The theoretical results are normalized to the value at 10.6 μm and plotted as the solid curve in Figure 5. As a result of the behavior of the KBr refractive index, the backscatter curve is essentially flat and therefore forms a good system calibration baseline. The triangles in the figure denote our measured backscatter data from KBr aerosols. These data are also normalized to the value at 10.6 μm.

The experimental data and theoretical curve are in excellent agreement. Our detection system response is essentially flat to within experimental error in the 9- to 11-μm region. Consequently, all of our biological aerosol backscattering data are presented assuming a flat system response.

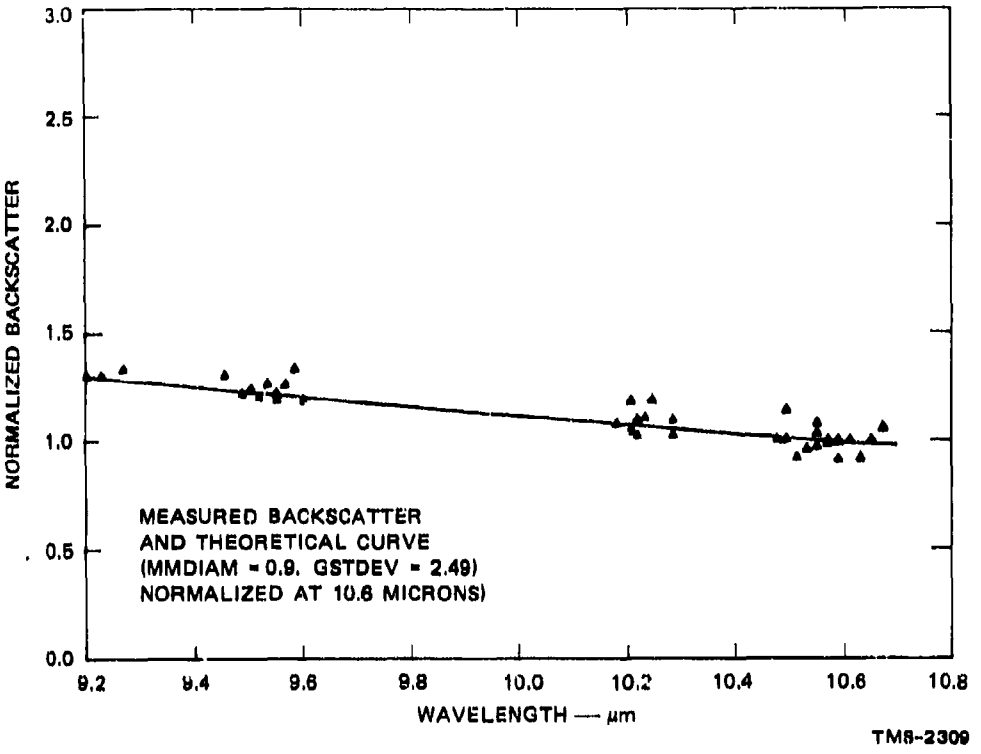

FIGURE 6 NORMALIZED IR BACKSCATTER FROM KBr AEROSOL

b. Backscatter Measurements

We measured backscatter from two different concentrations of B. subtilis spores, initially from a 0.1% solution, and later from a 0.3% solution in the syringe pump. The aerosols generated for the 0.1% solution were measured with the cascade impactor as log-normal with a 1.15-μm MMD and a geometric standard deviation of 2. Theoretical calculations were performed using our Mie code, the measured size distributions, and the complex refractive indices. The theoretical results are plotted as solid curves in Figures 6 and 7 with the experimental backscatter data. All curves are normalized to the value at 10.6 μm. The backscatter data measured from the 0.1% solution aerosol (Figure 6) show a slight discrepancy from the theoretically predicted curve. Since the data are normalized in the 10-μm region, any deviations will appear to be in the 9-μm region. With a higher aerosol concentration (Figure 7), the experimental and theoretical signatures are in excellent agreement.

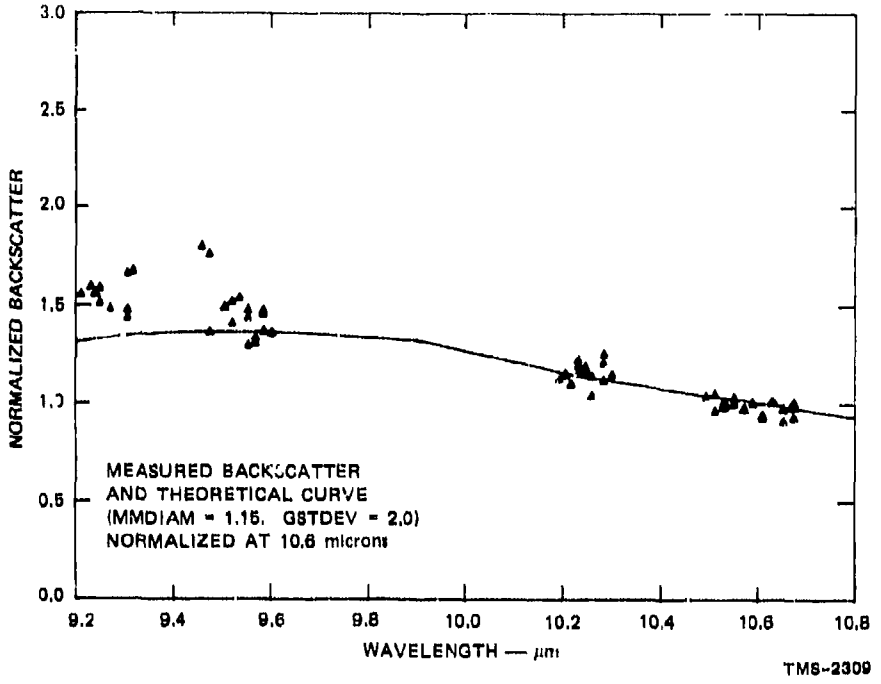

FIGURE 6 NORMALIZED IR BACKSCATTER FROM *B. SUBTILIS* SPORES AEROSOL (0.1% concentration)

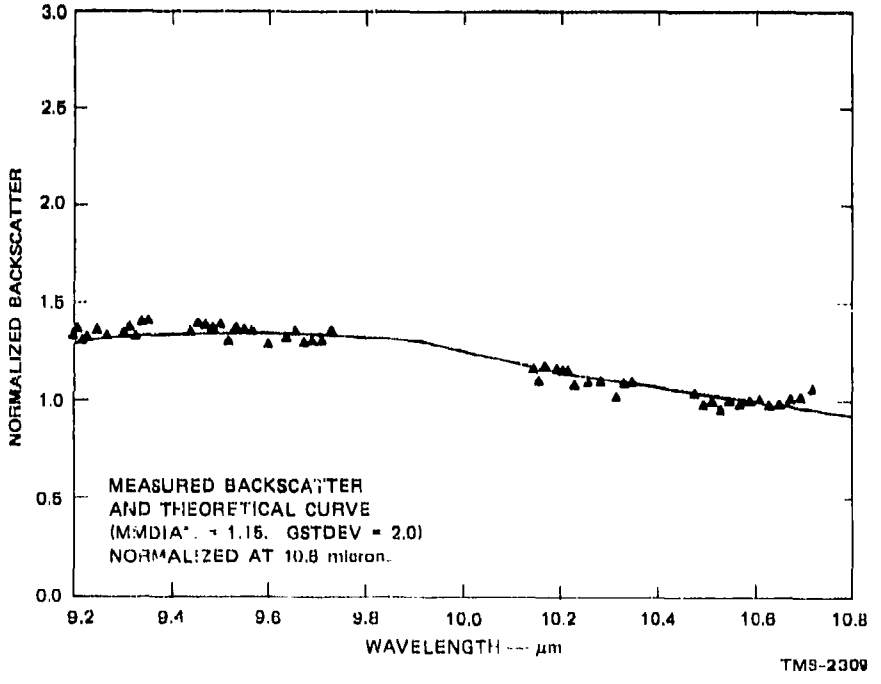

FIGURE 7 NORMALIZED IR BACKSCATTER FROM *B. SUBTILIS* SPORES AEROSOL (0.3% concentration)

Similarly, backscatter measurements from 0.1% and 0.3% solutions of M. luteus aerosol show deviation of the experimentally measured values from the theoretically computed values for the lower concentration. Figures 8 and 9 show data for the 0.1% and 0.3% solutions, respectively, of M. luteus aerosol. The theoretical values were computed from a measured size distribution and the complex refractive indices. Increasing the particle number density as shown in Figure 9 resulted in good agreement between theoretical and experimental values. The backscatter from the lower concentration solutions is quite small and results in a low signal-to-noise ratio (SNR) in the aerosol data. This can be observed in the amount of scatter in the data in Figures 6 and 8. However, the systematic deviation of the experiment from the theory in the 9-μm wavelength region may be due to an impure mode structure of the waveguide laser used in the low-concentration experiments. Subsequent measurements on the higher concentration aerosols were performed using a low-pressure discharge CO_2 laser, which exhibited a much cleaner mode structure than the waveguide CO_2 laser.

We also measured backscatter from aerosol samples of the vegetative form of B. subtilis. The experimental data are compared in Figure 10 with the theoretical curve generated as before, using measured size distributions. Due to the limited amount of material available, we used a 0.1% syringe pump solution concentration, which resulted in a weak backscatter signal. The large amount of scatter in the data is due to the resulting small SNR.

3. IR DISC Sensitivity Limits

The IR backscatter data measured for B. subtilis spores, B. subtilis, and M. luteus are consistent with the predictions of Mie theory when the measured complex refractive indices appropriate to the material and the measured aerosol size distributions are used as input. In the spectral region considered, the IR backscatter is relatively insensitive to the shape of the particles. The Mie predictions, which assume spherical particles, work equally well for B. subtilis (prolate

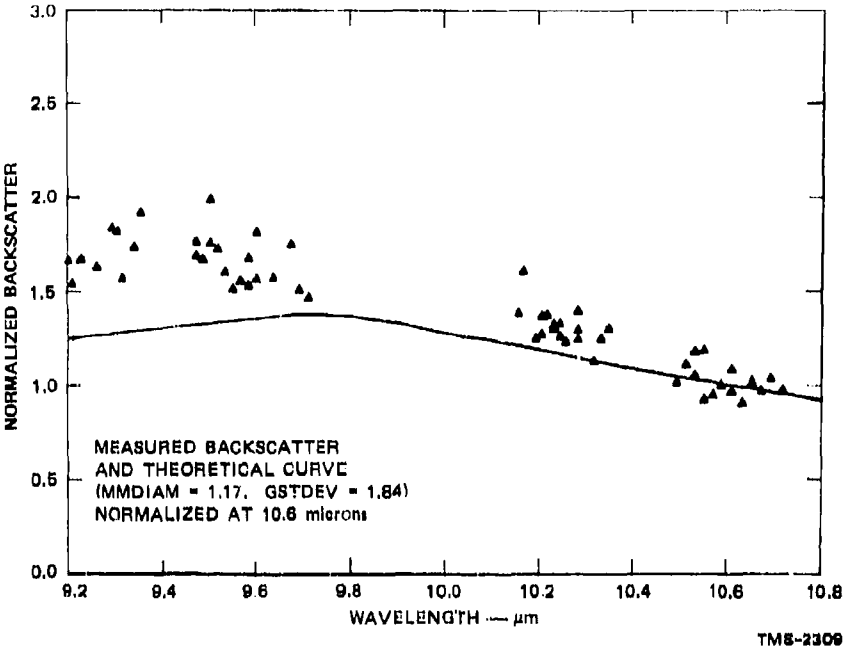

FIGURE 8 NORMALIZED IR BACKSCATTER FROM *M. LUTEUS* AEROSOL (0.1% concentration)

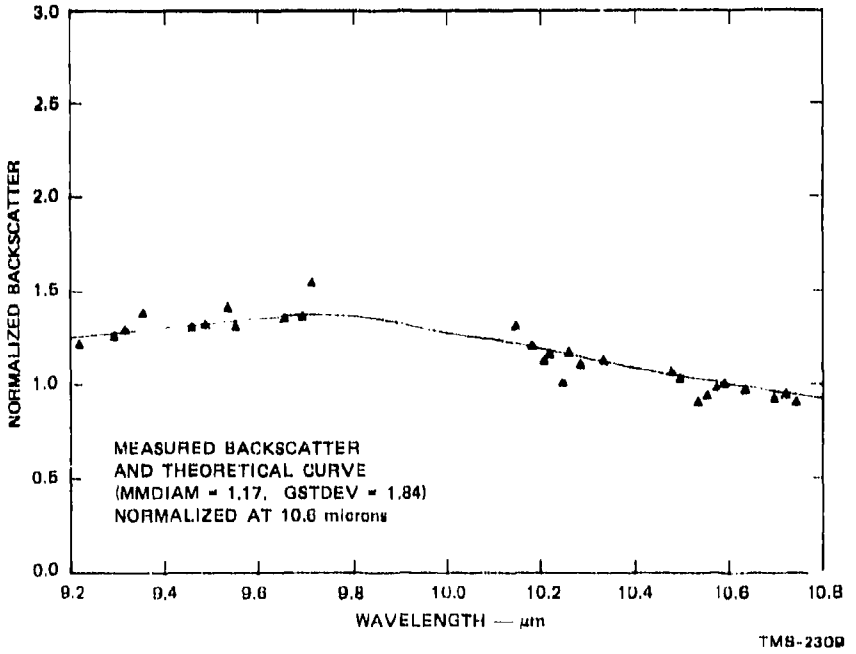

FIGURE 9 NORMALIZED IR BACKSCATTER FROM *M. LUTEUS* AEROSOL (0.3% concentration)

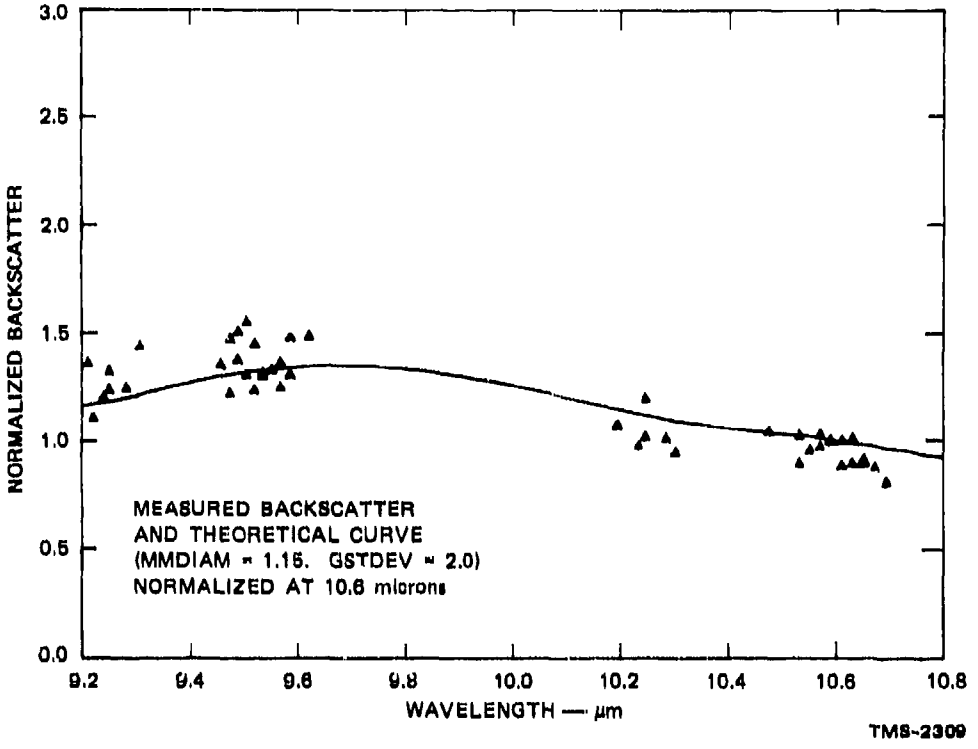

FIGURE 10 NORMALIZED IR BACKSCATTER FROM *B. SUBTILIS* AEROSOL

ellipsoid, bacilli) and M. luteus (spherical, coccoi). As illustrated in Figure 11 for B. subtilis spores, the backscatter curves are also relatively insensitive to the actual aerosol size distribution considered. We also note that the 9- to 11-μm backscatter signatures for aerosols of these materials do not exhibit distinctive features that might be used for DISC detection.

The latter point has significant implications for IR DISC sensitivity limits. As derived in Appendix A from the lidar equation, the difference in received power between two laser wavelengths, $P_r(\lambda_1)$ and $P_r(\lambda_2)$, is related to the atmospheric volume backscattering coefficient, β_π^{bok}, and the target aerosol backscatter cross section, σ_π^{bok}, by:

$$\frac{P_r(\lambda_1) - P_r(\lambda_2)}{P_r(\lambda_1) + P_r(\lambda_2)} = \frac{N\Delta\sigma_\pi + \Delta\beta_\pi^{bok}}{2N\bar{\sigma}_\pi + 2\bar{\beta}_\pi^{bok}} \quad , \tag{1}$$

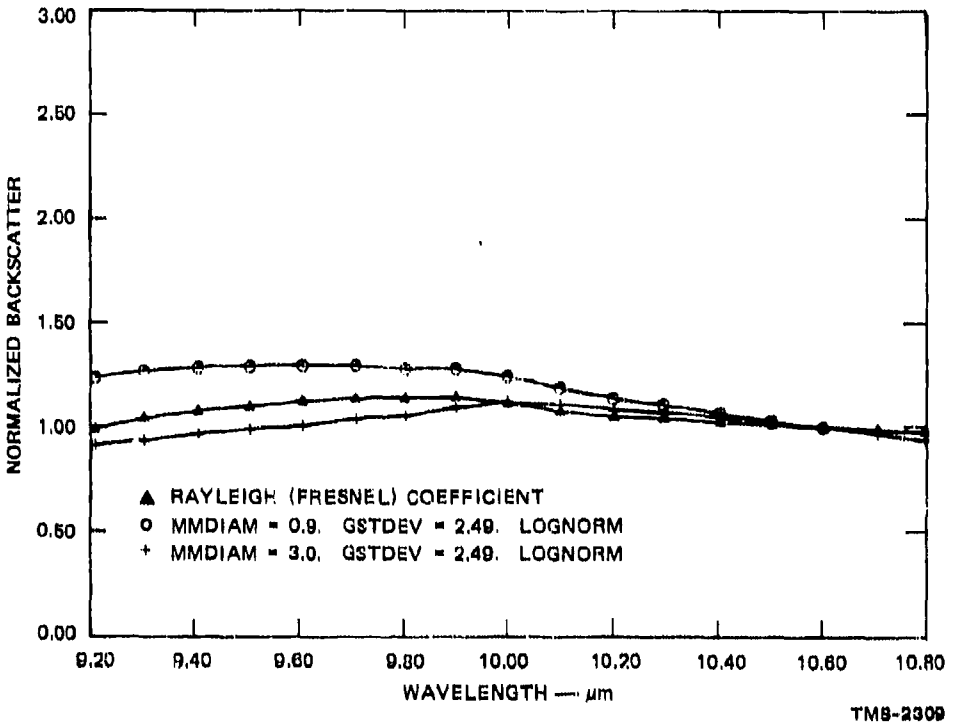

FIGURE 11 EFFECT OF SIZE DISTRIBUTION ON IR BACKSCATTERING FROM *B. SUBTILIS* SPORES AEROSOLS

where $P_r(\lambda_n)$ is the power received from the backscatter of wavelength λ_n, and N is the target aerosol number density. Since the backscatter coefficient for biological aerosols varies slowly with wavelength, a significant differential backscatter requires at least 1 μm difference between two probing wavelengths in the 8- to 11-μm region. Over this wavelength interval, the atmospheric volume backscattering coefficient changes significantly (typically $\sim 10^{-8}$ $m^{-1}sr^{-1}$). From the lidar equation, the backscatter terms are comparable when

$$N\Delta\sigma_\pi \sim \Delta\beta_\pi^{bak} \quad . \tag{2}$$

For a distribution of B. subtilis spores with a MMD of 3 μm and a density of 1 particle/cc, the differential backscatter is approximately 10^{-10} $m^{-1}sr^{-1}$, or two orders of magnitude less than the differential atmospheric volume backscatter coefficient. Thus, an IR DISC system can detect the presence of biological aerosols only if the number density exceeds 100 particles/cc, or 10^5 particles/liter. Considering that the U.S. Army's biological aerosol particle detection sensitivity goal is in the range of 5 to 10 particles/liter, we concluded that IR DISC is not a viable technique for remote detection of biological aerosols. Therefore, we deleted the IR DISC work and began to study the CIDS technique, which appeared to be more promising for meeting the Army's stated detection sensitivity goals. The CIDS concept was investigated for the remainder of the contract.

B. Circular-Intensity Differential Scattering (CIDS)

The CIDS technique can achieve better sensitivity than IR DISC in detecting biological aerosols because it minimizes or eliminates the differential signal from the natural aerosol background. CIDS is the differential scattering of left and right circularly polarized light, which, in biological materials, results from the chiral, or helical, structures of biological macromolecules, primarily DNA. CIDS is sensitive to the relationship of the pitch, radius, and length of the helical structures to the wavelength of the probing light.[3-6] Because the natural aerosol background consists mainly of optically inactive, inorganic dust particles, the interfering differential signal from this background is essentially eliminated when the CIDS technique is used.

The CIDS signal is defined as

$$S = \frac{I_L(\theta) - I_R(\theta)}{I_L(\theta) + I_R(\theta)} \quad , \tag{3}$$

where θ is the scattering angle and I_L and I_R are, respectively, the scattering intensities for left and right circularly polarized incident light. Based on some preliminary work at Los Alamos,[7-8] it is believed that CIDS spectra can provide unique signatures for the identification of microorganisms and the magnitude of typical signals in the 300- to 600-nm spectral region range from 10^{-3} (for viruses) to 10^{-4} (for bacteria).

The IR DISC lidar system discussed in Appendix A can be easily modified to measure CIDS. To accomplish this, rather than transmitting two laser pulses at different wavelengths (λ_1, λ_2) and measuring the differential backscatter, one transmits two pulses at the same wavelength but in different circular polarization states (λ_L, λ_R) and measures the differential backscatter. Following the analysis of Appendix A, one obtains the same result for the differential signal,

$$S = \frac{N(R)\,\Delta\sigma_\pi + \Delta\beta_\pi^{bak}(R)}{2N(R)\,\bar{\sigma}_\pi + 2\bar{\beta}_\pi^{bak}(R)} \quad . \tag{4}$$

However, in the CIDS case,

$$\Delta\sigma_\pi = \sigma_\pi(\lambda_L) - \sigma_\pi(\lambda_R),$$

$$\Delta\beta_\pi^{bak}(R) = \beta_\pi^{bak}(R, \lambda_L) - \beta_\pi^{bak}(R, \lambda_R),$$

$$\bar{\sigma}_\pi = \tfrac{1}{2}[\sigma_\pi(\lambda_L) + \sigma_\pi(\lambda_R)], \text{ and}$$

$$\bar{\beta}_\pi^{bak}(R) = \tfrac{1}{2}[\beta_\pi^{bak}(R, \lambda_L) + \beta_\pi^{bak}(R, \lambda_R)].$$

The advantage over IR DISC is that one expects the CIDS from the optically inactive natural aerosol, $\Delta\beta_\pi^{bak}(R)$, to be essentially zero. Hence, the signal reduces to

$$S = \frac{N(R)\,\Delta\sigma_\pi}{2N(R)\,\bar{\sigma}_\pi + 2\bar{\beta}_\pi^{bak}(R)} \quad , \tag{5}$$

which is a measure only of the CIDS-active biological particles. Note also that in a CIDS measurement the atmospheric extinction factor in Equation (A-3) in Appendix A can be rigorously set to unity, i.e.,

$$\Delta k_{ext}(r) = k_{ext}(r, \lambda_L) - k_{ext}(r, \lambda_R) = 0,$$

since natural atmospheric aerosols and gases generally will not differentially absorb or scatter left and right circularly polarized light.

Based on these considerations, SRI proposed to discontinue the IR DISC studies and concentrate on CIDS in the final year of this project. We proposed initially to measure CIDS from liquid suspensions of biological microorganisms over the 300- to 600-nm spectral region at fixed scattering angles of 90° and 180°. If the spectra appeared to provide a unique signature of the microorganisms, we would then proceed with backscattering measurements of biological aerosols using the aerosol chamber. SRI received permission from ARO to proceed with this work in September of 1984.

1. Experimental Method

Two methods exist for collecting CIDS spectra on liquid suspensions of microorganisms. The first method uses a fixed-frequency light source, usually a laser, and measures CIDS as a function of scattering angle. The second method fixes the scattering angle and measures CIDS as a function of the wavelength of the incident light. We chose the latter for our studies since it is the only method that can be implemented in a single-ended (backscattering) system for in-situ monitoring of biological aerosol clouds.

Figure 12 is a schematic diagram of the system SRI constructed, set up for 90° scattering. A 300-W xenon light source illuminates the entrance slit of a scanning monochrometer. The slit width (2 mm) is chosen to yield approximately a 4-nm bandpass over the 300- to 600-nm spectral region. Light from the monochrometer exit slit is linearly

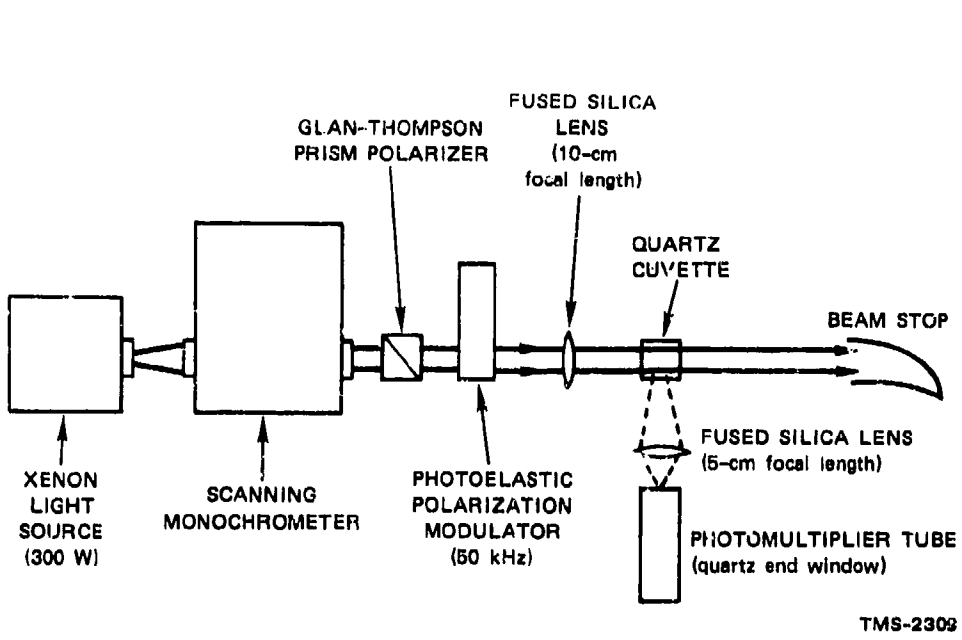

FIGURE 12 OPTICAL SCHEMATIC OF CIDS SPECTROMETER CONFIGURED FOR 90° MEASUREMENTS

polarized at +45° by a Glan-Thompson prism polarizer and directed through a photoelastic polarization modulator[9] that acts as a 50-kHz periodically varying retardation plate. As a result, the polarization state of the light emerging from the modulator alternates between left and right circular at a 50-kHz rate. This polarization-modulated light is next focused by a fused silica lens into a quartz cuvette containing a suspension of the material under investigation. Light scattered at 90° is collected by a second fused silica lens and focused onto the photocathode of a photomultiplier (PMT) tube with a quartz end window. If the suspension of particles differentially scatters left and right circularly polarized light, the photocurrent will contain a 50-kHz component that is phase-sensitively detected using a lock-in amplifier referenced to the modulator.

CIDS spectra are obtained by measuring the ratio of the lock-in output to the average PMT photocurrent and recording the resultant signal on a chart recorder driven synchronously with the scanning monochrometer. During a spectral scan, the PMT voltage is adjusted by an active circuit to maintain a nearly constant average photocurrent.

To check our CIDS spectrometer for measurement artifacts, we recorded spectra at both 90° and near-180° from liquid suspensions of polystyrene microspheres. Since polystyrene microspheres are optically inactive, they should not give rise to a CIDS signal. Figure 13 shows the signal obtained from a suspension of 0.087-μm polystyrene microspheres in water at a concentration of $\sim 10^{11}$/cc. The signal varies monotonically from $+6 \times 10^{-3}$ at 350 nm to $+3 \times 10^{-3}$ at 600 nm. The origin of this relatively large artifact signal is the linear birefringence associated with the cuvette windows and fused silica focusing lens. We have found that rotating the cuvettes to expose new entrance and exit faces, changing sample cuvettes, or changing the focusing lens will change the overall magnitude of this artifact signal, but not its shape as a function of wavelength.

The magnitude and shape of the observed signal also depends on polystyrene particle size. Figure 14 shows the backscattering signal obtained from a suspension of 1.09-μm polystyrene microspheres. The curve exhibits a pronounced series of maxima and minima and varies in magnitude from $+5 \times 10^{-5}$ at 350 nm to $+3 \times 10^{-4}$ at 600 nm. This curve looks just like the normal Mie scattering from 1.09-μm polystyrene microspheres. The shape of the curve is qualitatively different from the one obtained for the 0.087-μm spheres and its maximum signal is about an order of magnitude smaller.

For a given particle size, we find that the shapes of the artifact spectra are similar for both 90° and near-180° scattering. However, the magnitudes of the measured signals are quite different. Typically, the near-180° signal is one to two orders of magnitude smaller than the 90° signal at any given wavelength.

All of these features of the observed artifact spectra can be explained by a careful analysis of the Stokes vector of the light beam as it propagates through the various polarization-sensitive elements in our CIDS spectrometer. This detailed analysis is presented in Appendix B, which concludes that the artifact signal is caused by a mixing of (1) the residual linear birefringence in any optical materials placed

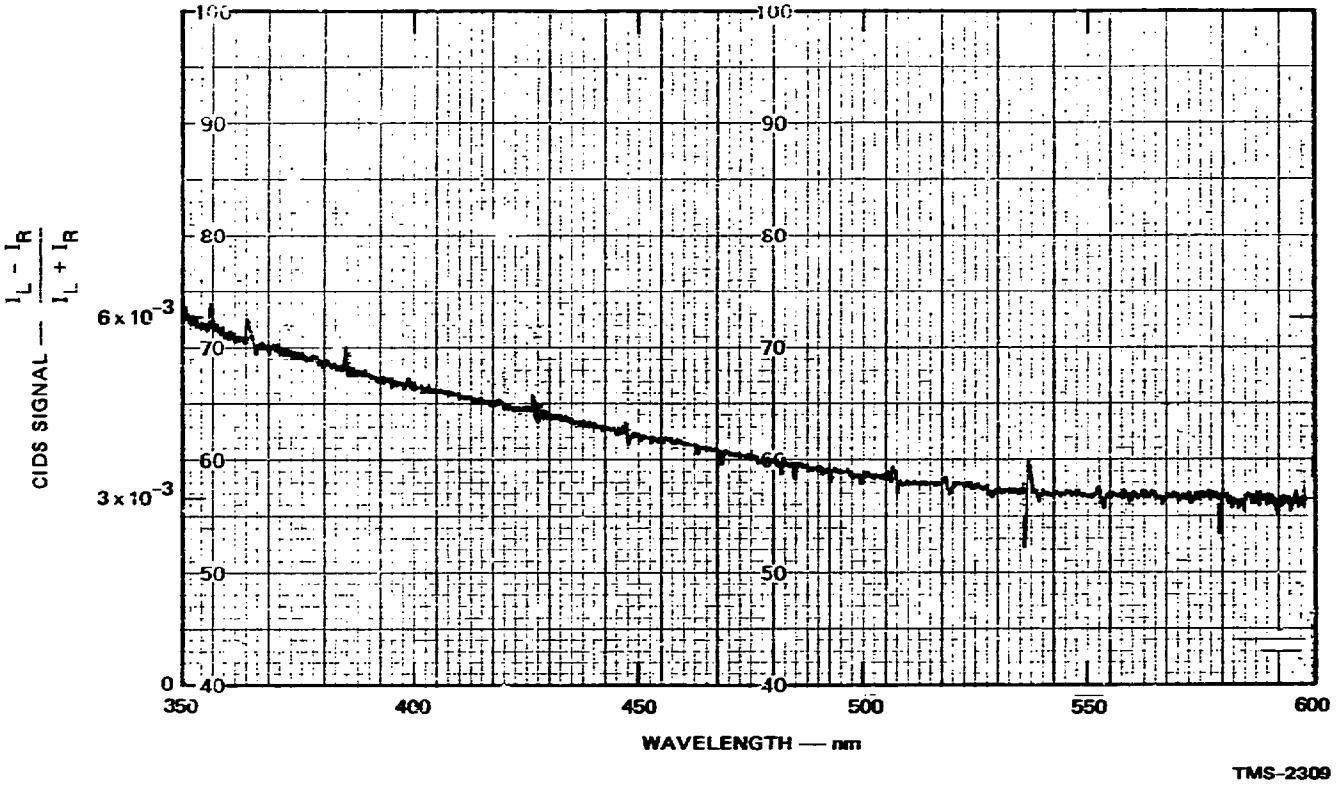

FIGURE 13 ARTIFACT CIDS SIGNAL FROM A LIQUID SUSPENSION OF 0.087-μm POLYSTYRENE MICROSPHERES

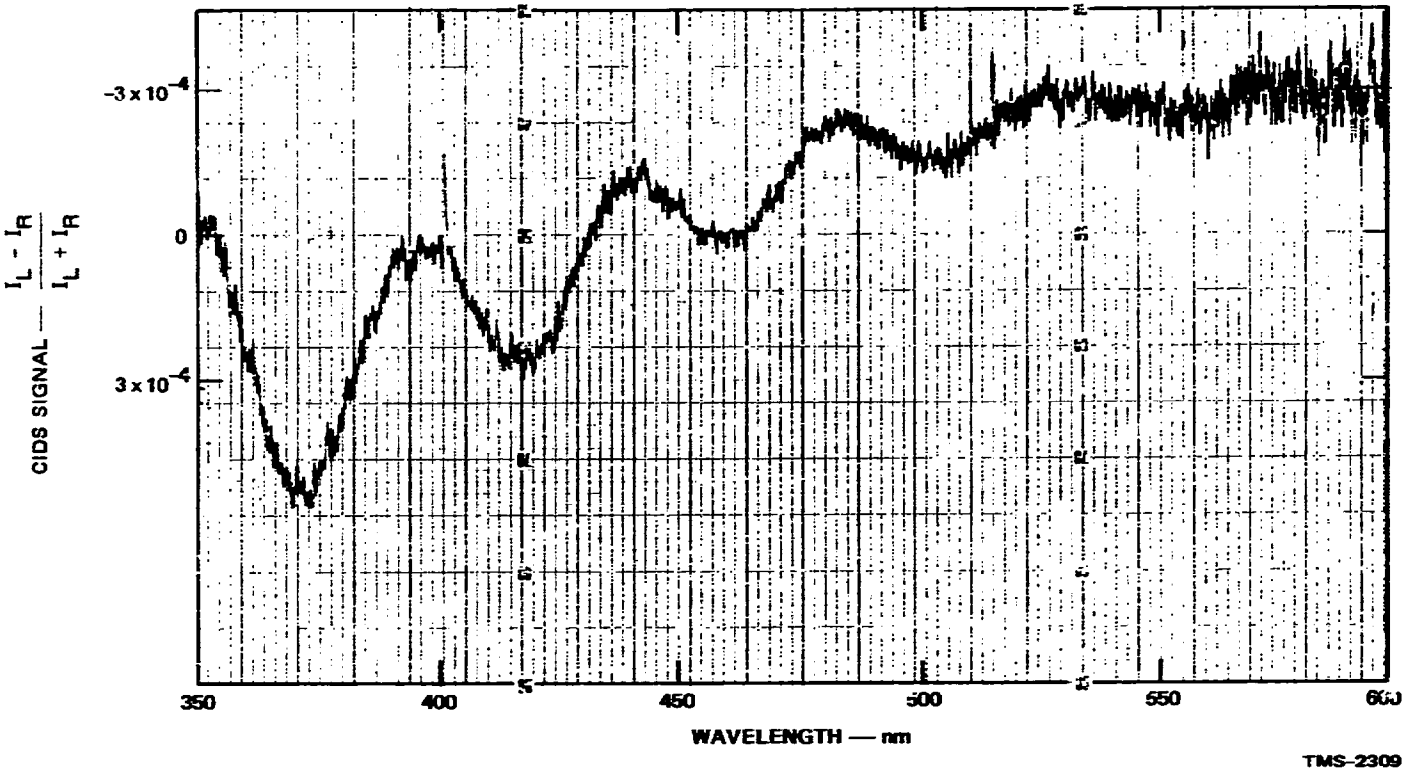

FIGURE 14 ARTIFACT CIDS SIGNAL FROM A LIQUID SUSPENSION OF 1.09-μm POLYSTYRENE MICROSPHERES

between the photoelastic modulator and the scattering solution, and (2) the normal Mie scattering of the particle suspension. In the configuration of Figure 12, these optical materials include both the focusing lens and the cuvette entrance window. Appendix B also explains why the artifact spectra are essentially just Mie scattering from the 1.09-μm and 0.087-μm microsphere suspensions, and why the 90° signal is much larger than the near-180° signal in each case.

2. CIDS Spectra from Suspensions of Microorganisms

The Stokes vector analysis of our CIDS spectrometer discussed in Appendix B is extended in Appendix C to cover the case in which the scattering suspension consists of biological microorganisms. This analysis shows that the 50-kHz component of the detector photocurrent measured by our instrument is a mixture of CIDS from the biological suspension and linear birefringence from the cuvette entrance window and focusing lens. Hence, for these measurements, it is important to select focusing lenses and cuvettes with a minimum of linear birefringence. In our 90° scattering experiments we found that we could eliminate the fused silica focusing lens entirely by simply moving the cuvette as close to the modulator as possible. In the near-180° scattering experiments, the light beam was focused using a spherical mirror with the cuvette located ~12° off-axis. This configuration is illustrated in Figure 15. Hence, in our experiments the limiting source of linear birefringence is the cuvette entrance window. However, we were unable to obtain quartz cuvettes with windows having no measurable linear birefringence, and therefore selected, out of six cuvettes, two having the minimum window birefringence, and used only these in our subsequent experiments.

We measured CIDS spectra at scattering angles of 90° and 168° from suspensions of T2 and T4 viruses and from E. coli in phosphate-buffered saline solutions. The viral samples were obtained in lyophilized form from American Type Culture Collection (ATCC) and dispersed in solution as needed. The E. Coli (ATCC 14948) were grown in standard tryptic soy

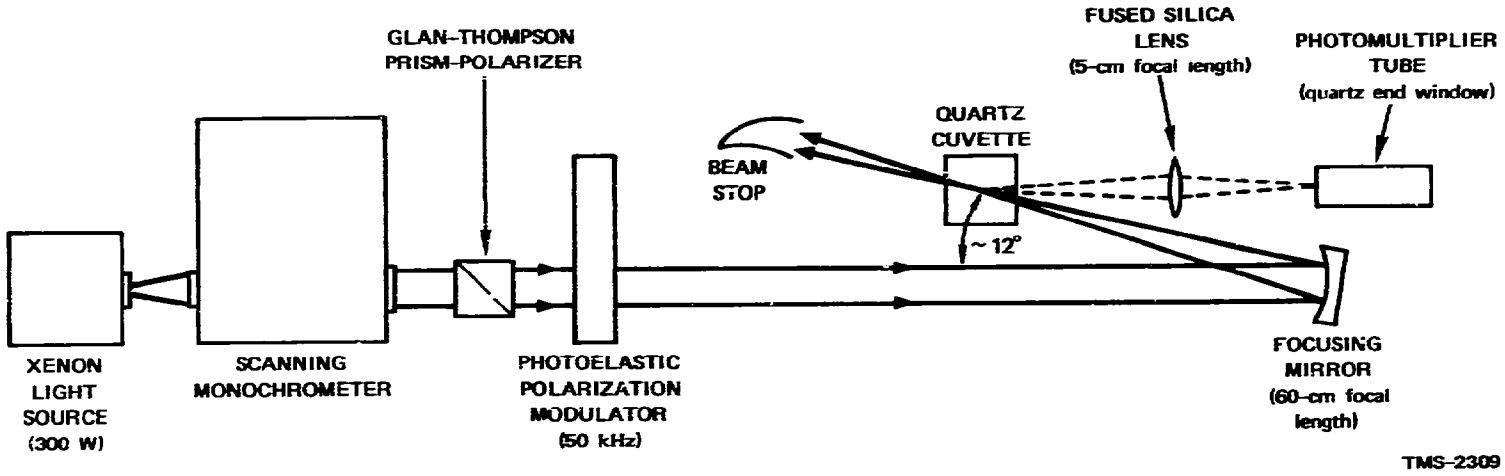

FIGURE 15 OPTICAL SCHEMATIC OF CIDS SPECTROMETER CONFIGURED FOR NEAR 180° MEASUREMENTS

broth (Difco), harvested by continuous centrifugation, washed with deionized water, and then dispersed in solution. We were unable to collect data on suspensions of microorganisms in their growth media because the relatively strong fluorescence exhibited by the growth media always greatly exceeded the elastically scattered light from the suspended particles. We therefore performed all CIDS measurements from supervisons in phophate-buffered saline, which is non-fluorescent. Reference spectra were obtained from suspensions of polystyrene microspheres in water in the same quartz cuvettes used to measure CIDS from the biological suspensions. High-concentration samples were required in our experiments because of the relatively low intensity in our incident light beam (typically $I_o \approx 100$ μW). Use of a brighter light source would allow for measurements on samples of much lower concentration.

Figure 16 shows the 90° CIDS from Sample 1, a suspension of T2 virus of concentration 1.5×10^{10}/cc (top curve) and the 90° CIDS artifact from a suspension of 0.087-μm polystyrene microspheres at a concentration of 10^{10}/cc (bottom curve). The 0.087-μm spheres were chosen as a reference because they approximate the actual size of the T2 virus particles (viral head ~600 Å in diameter, tail ~1000 Å in length). These measurements were performed using the same cuvette in the same orientation (i.e., with the same entrance and exit windows), and the scan in wavelength is from 350 nm to 600 nm. The T2 CIDS is clearly distinguishable from the artifact spectrum.

Figure 17 shows the artifact curve and CIDS spectrum from Sample 2, a suspension of T2 virus at a lower concentration (~5×10^9/cc). Again, both the artifact and CIDS spectra were taken from the suspensions in the same quartz cuvette in the same window orientation. As was the case with the first sample, the T2 spectrum is clearly distinguishable from the artifact spectrum. In addition, it is different from the T2 CIDS recorded from the first sample. Since CIDS is, in principle, independent of concentration, we should have obtained the same spectrum from the two T2 samples. The reason we did not is, we believe, due to the fact that the higher concentration sample was quite turbid and exhibited

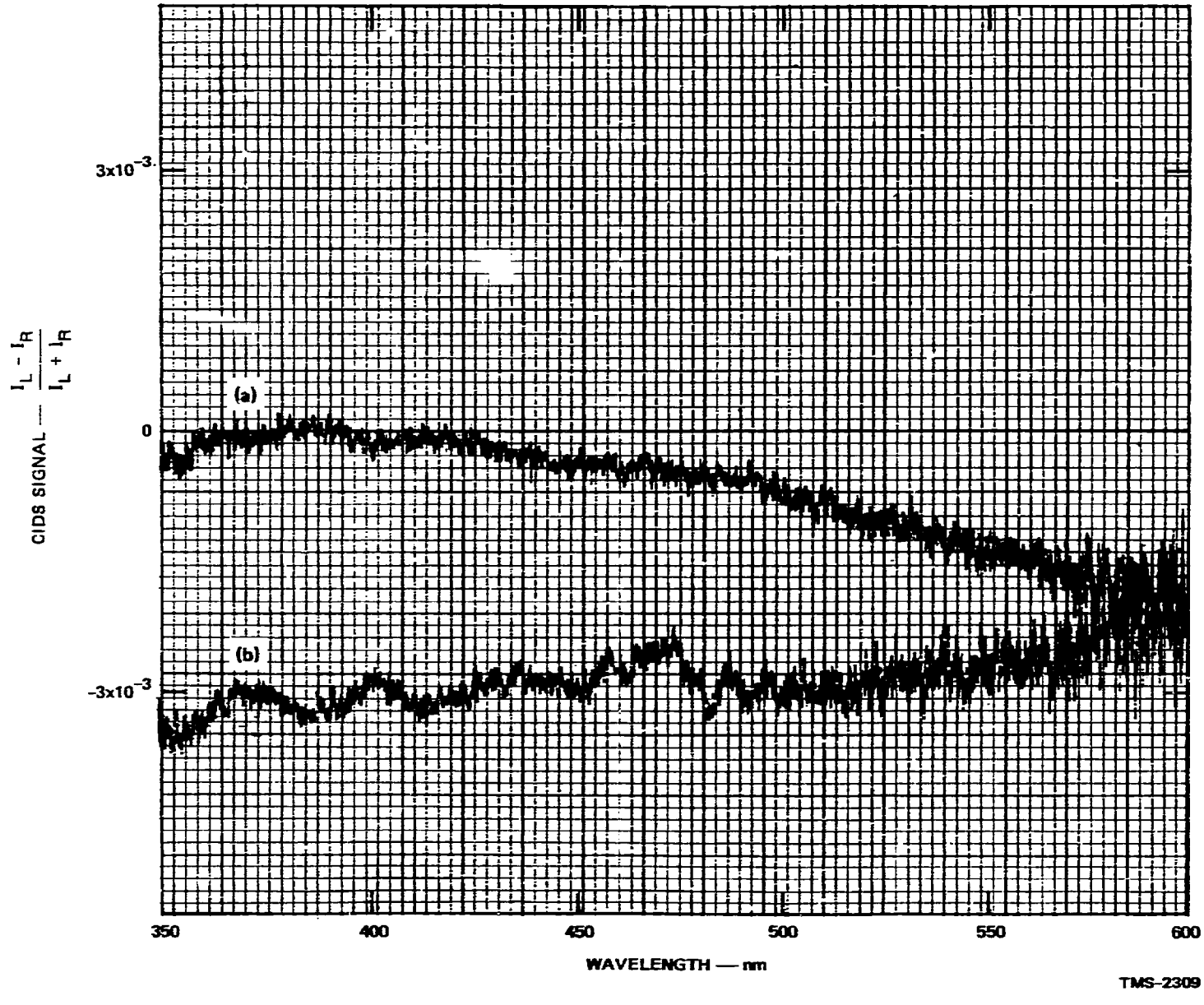

FIGURE 16 (a) 90° CIDA SPECTRUM FROM T2 VIRUS SUSPENSION SAMPLE 1 (concentration 1.5 x 10^{10}/cc); (b) ARTIFACT SPECTRUM FROM 0.087-μm POLYSTYRENE MICROSPHERES

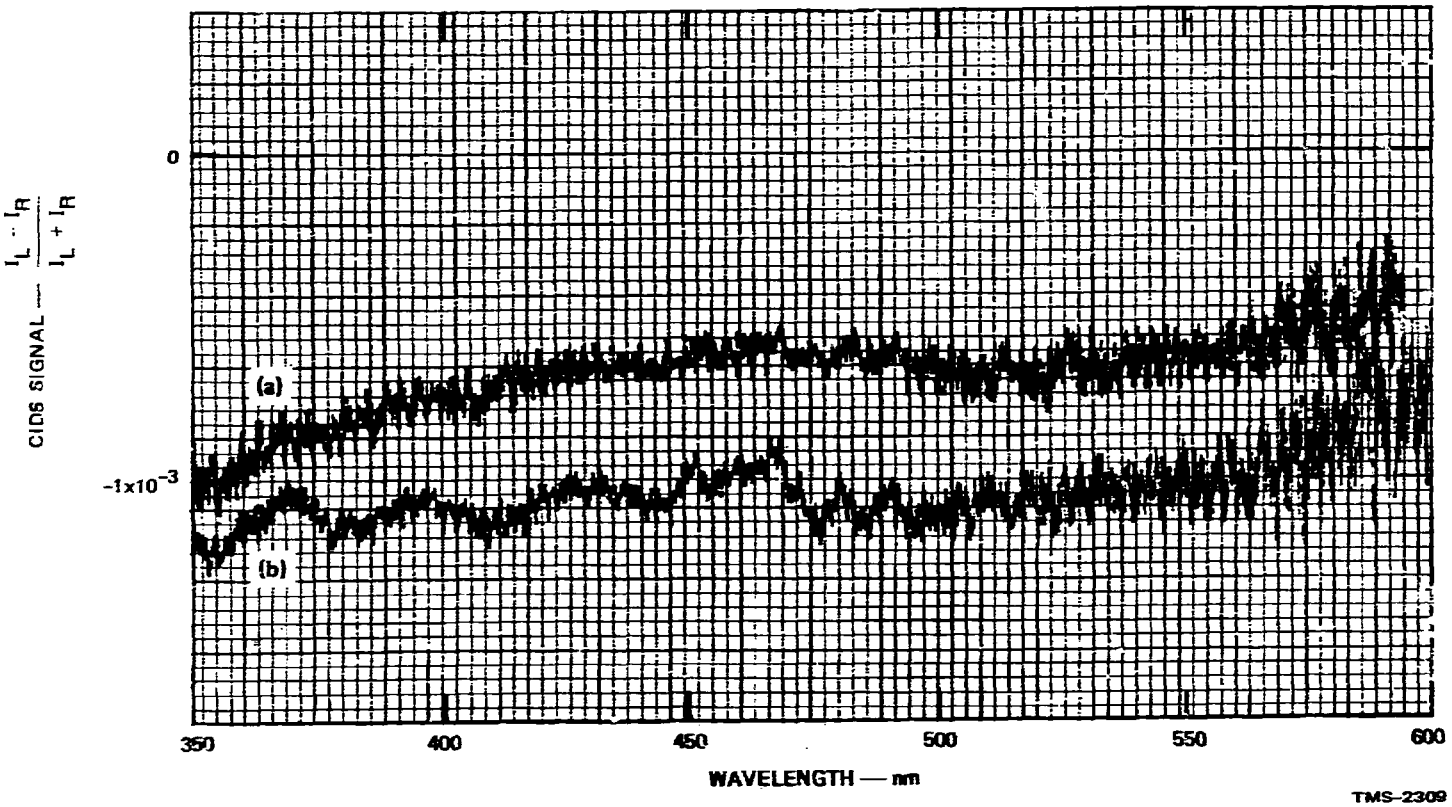

FIGURE 17 (a) 90° CIDS SPECTRUM FROM T2 VIRUS SUSPENSION SAMPLE 1 (concentration 5 x 10^9/cc); (b) ARTIFACT SPECTRUM FROM 0.087-μm POLYSTYRENE MICROSPHERES

a significant degree of multiple scattering. CIDS measurements on a lower concentration (~10^9/cc) T2 sample yielded essentially the same spectrum shown in Figure 17, demonstrating that this is in fact the correct single scattering CIDS spectrum from T2.

CIDS spectra were collected from these two T2 samples (Sample 1 with a concentration of ~1.5 x 10^{10}/cc, and Sample 2 with a concentration of ~5 x 10^9/cc) over a period of several days following their preparation to check reproducibility and record any changes. Although both samples were initially quite turbid, the turbidity decreased substantially over the course of several days, indicating a decrease in the concentration of the scattering particles. Figure 18 is the 90° CIDS spectrum from Sample 1 recorded two days after its preparation. Note that it is qualitatively different from its spectrum (Figure 16) recorded on the day of preparation, and similar to the spectrum first recorded from Sample 2 (Figure 17). Apparently, the decrease in turbidity of Sample 1 with time brought it into a single scattering regime. Figure 19 is the 90° CIDS spectrum from Sample 2 recorded one day after its preparation. For comparison, also plotted is the 90° artifact curve from 0.087-μm polystyrene microspheres. Note that the two curves are almost identical, and that the CIDS curve is qualitatively different from the one recorded for this sample on the day of its preparation (Figure 17). Apparently, the T2 virus particles lyse after approximately one day in the phosphate-buffered saline solution, and their protein skeletons are all that remain to scatter light. Since the protein skeletons are not helical structures (they contain no DNA) and are much smaller than the wavelength of light, they give an artifact signal essentially identical to that from the polystyrene microspheres. Thus, we are confident that the T2 90° CIDS spectrum shown in Figure 18 is in fact due to the DNA in the viral head.

CIDS spectra collected at 168° from these T2 suspensions are approximately one order of magnitude smaller than those obtained at 90°. The 168° CIDS from the T2 Sample 1 is shown in Figure 20. This curve is different from both the 90° CIDS curve and the 168° artifact

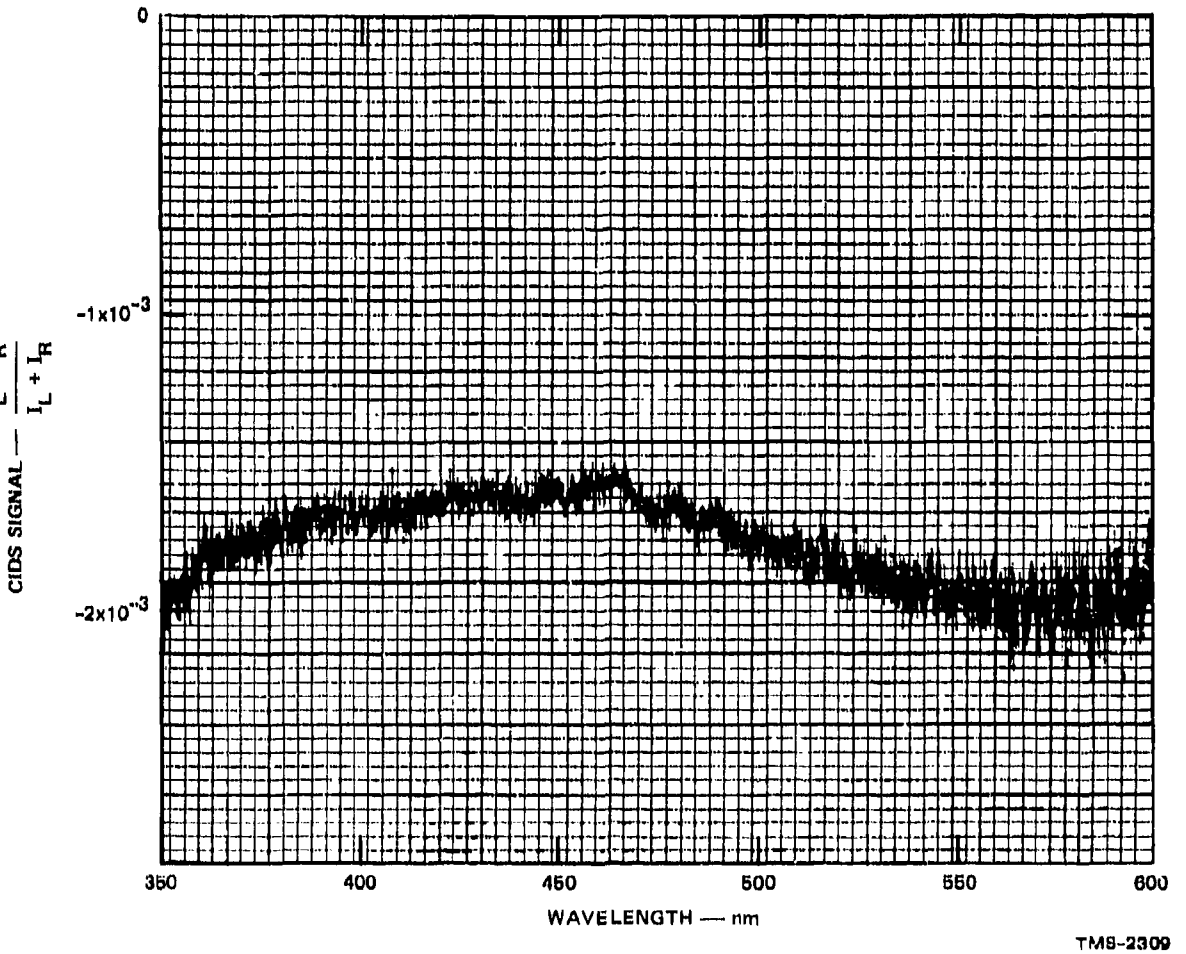

FIGURE 18 90° CIDS SPECTRUM FROM T2 VIRUS SUSPENSION (Initial concentration ~ 1.5 x 10^{10}/cc) RECORDED TWO DAYS AFTER PREPARATION

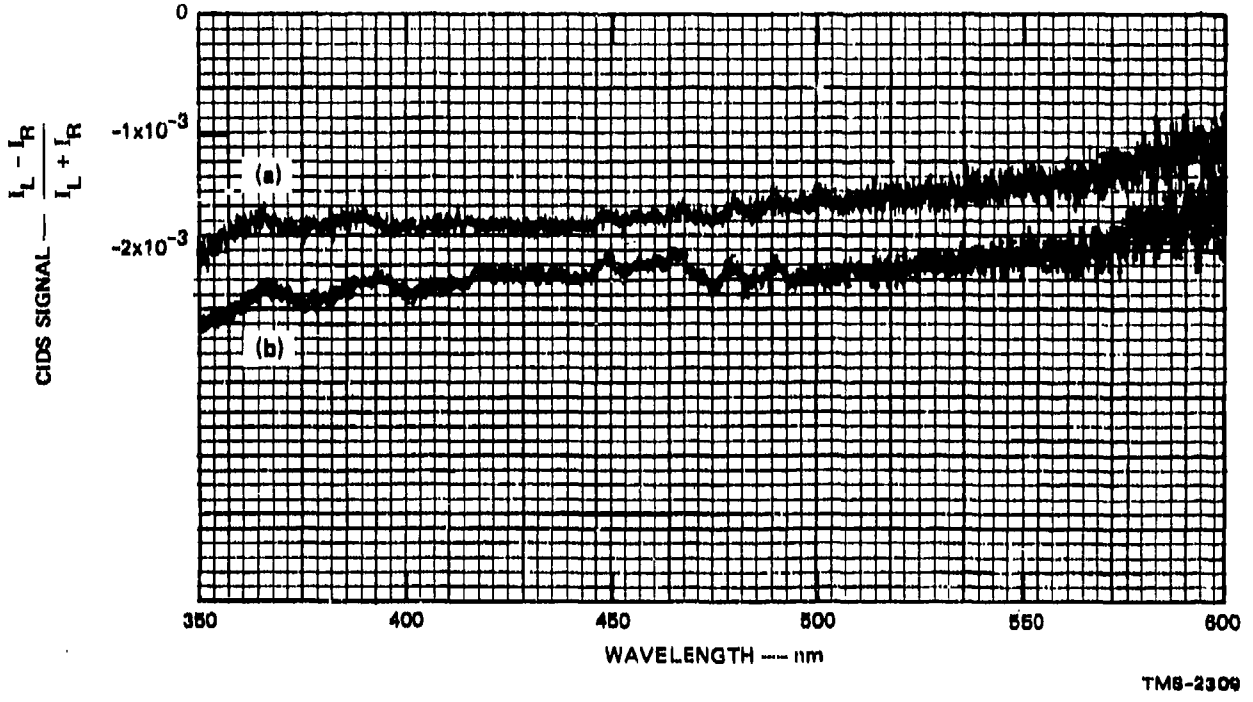

FIGURE 19 (a) 90° CIDS SPECTRUM FROM T2 VIRUS SUSPENSION (Initial concentration ~ 5 x 10^9/cc) ONE DAY AFTER PREPARATION; (b) ARTIFACT SPECTRUM FROM 0.087-μm POLYSTYRENE MICROSPHERES

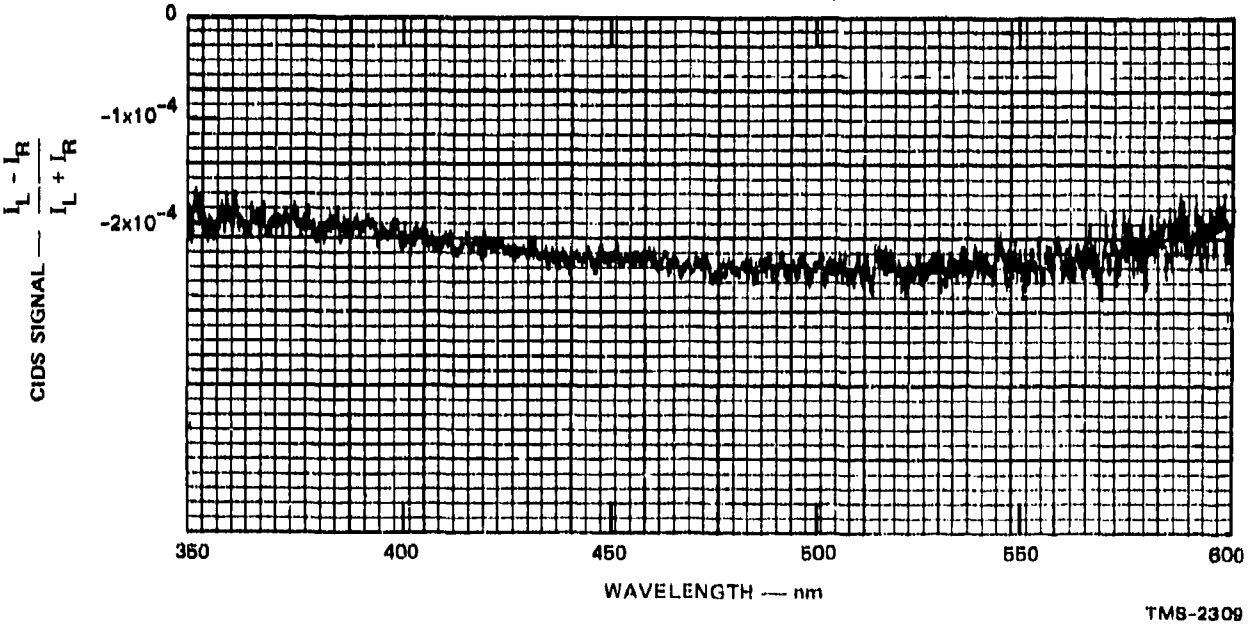

FIGURE 20 168° CIDS SPECTRUM FROM T2 VIRUS SUSPENSION (Sample 1)

curve from the polystyrene microspheres. The 168° CIDS from T2 is much less pronounced than the 90° curve and does not possess any significant spectral features that might be used for identification purposes.

Both 90° and 168° CIDS spectra were collected from similarly prepared samples of T4 virus in phosphate-buffered saline soultion. The spectra obtained were in all cases identical to those from the T2 suspensions and are therefore not presented here. This is not suprising since the only difference between the T2 and T4 DNA is the genetic code sequence, which does not affect the DNA chiral structure (i.e., DNA helix pitch, radius, and length), and therefore should not affect the CIDS.

CIDS spectra from suspensions of E. coli microorganisms concentration ($\sim 10^6$/cc) are shown in Figure 21 for 90° scattering and Figure 22 for 168° scattering. Note that the two spectra are qualitatively different from each other and from the T2 spectra. Again, the 168° signal is approximately one order of magnitude smaller than the 90° signal and exhibits a much less pronounced shape. For comparison, Figure 23 shows a 168° artifact spectrum from a suspension of 2.02-μm polyvinyl toluene microspheres. These were chosen because they approximate the actual size of E. coli bacteria.

3. Discussion and Conclusions

The CIDS spectra collected from the viruses T2 and T4 and the bacteria E. coli over the 350- to 600-nm region at scattering angles of 90° and 168° do not exhibit distinctive features which might be used for remote or local in-situ DISC detection. For example, the data collected from the T2 and T4 viruses are indistinguishable and relatively flat over the measurement spectral range. In fact, the artifact spectra from optically inactive suspensions of microspheres exhibited more interesting structure than the biological suspensions. Such artifact signals are expected to be present to some degree in any remote or local in situ optical sensor. We also note that the near-backscattering CIDS spectra from the microorganisms, which are the most relevant from the point of

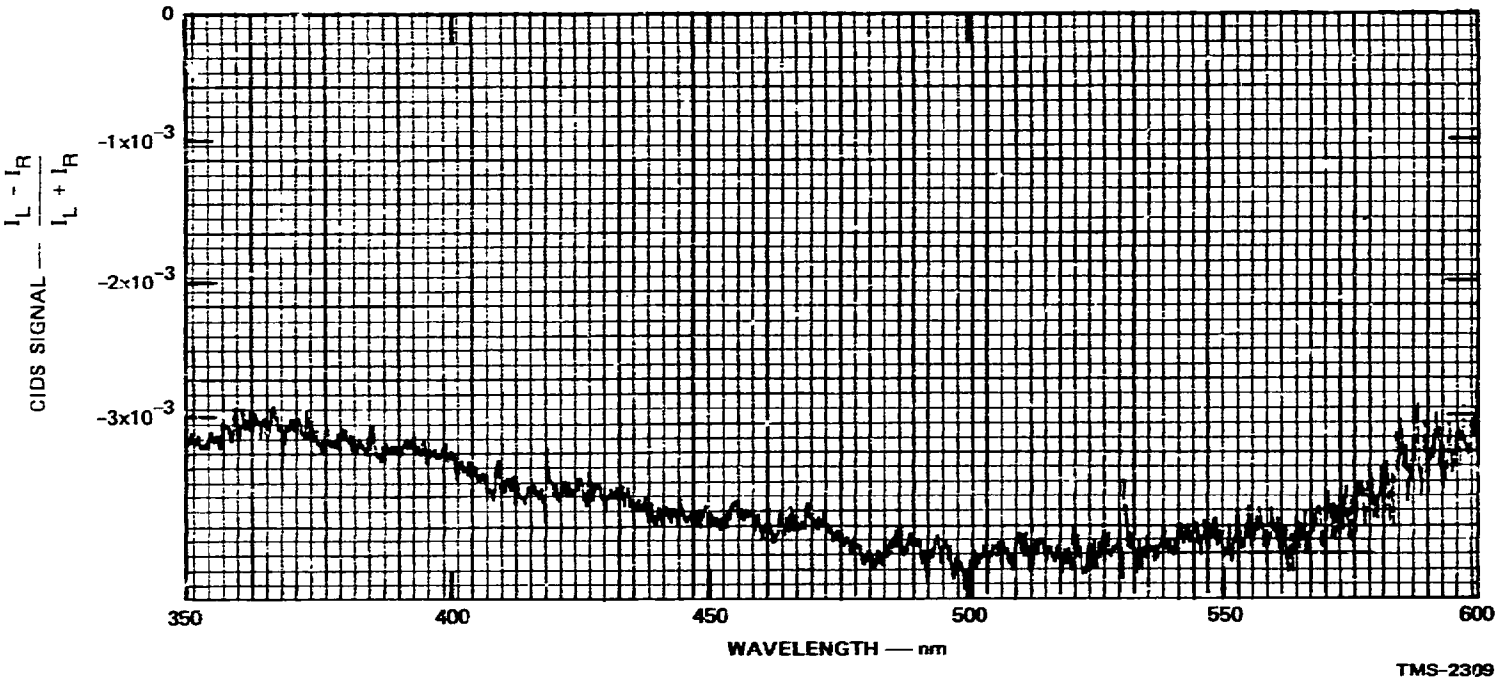

FIGURE 21 90° CIDS SPECTRUM FROM *E. COLI* SUSPENSION (concentration $\sim 10^6$/cc)

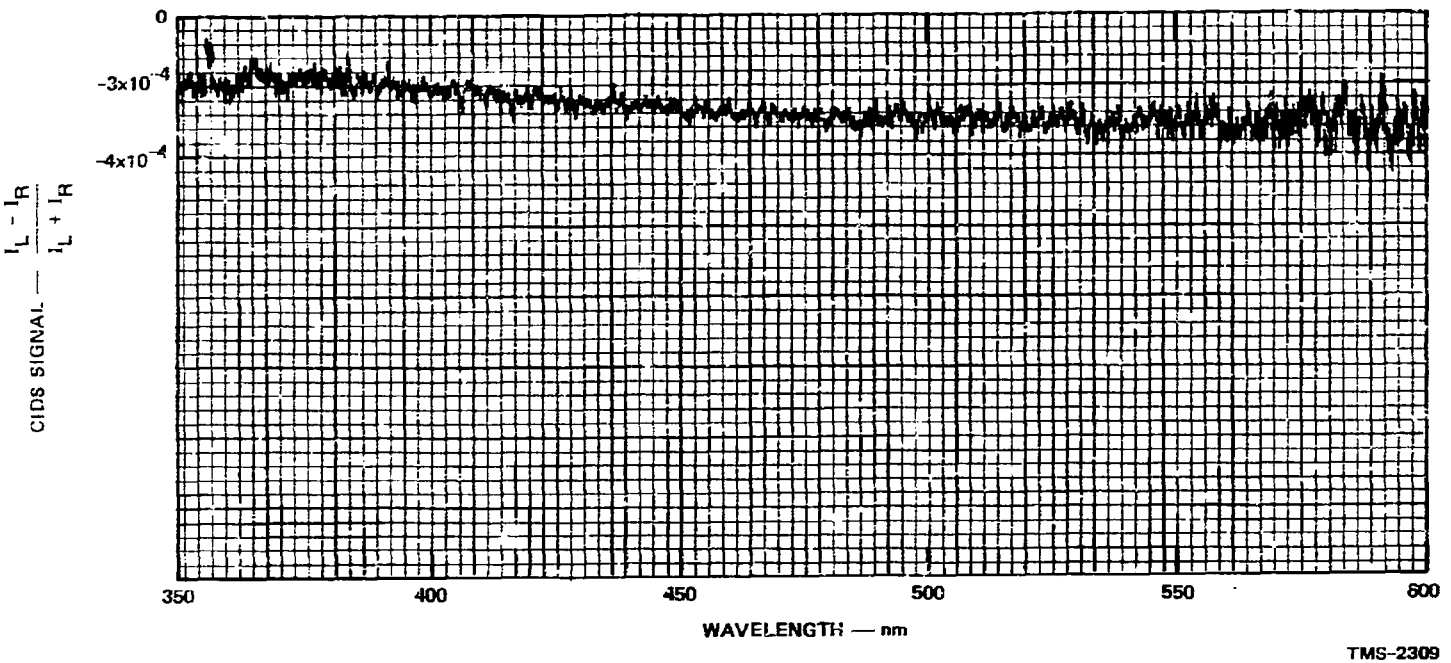

FIGURE 22 168° CIDS SPECTRUM FROM *E. COLI* SUSPENSION (concentration $\sim 10^6$/cc)

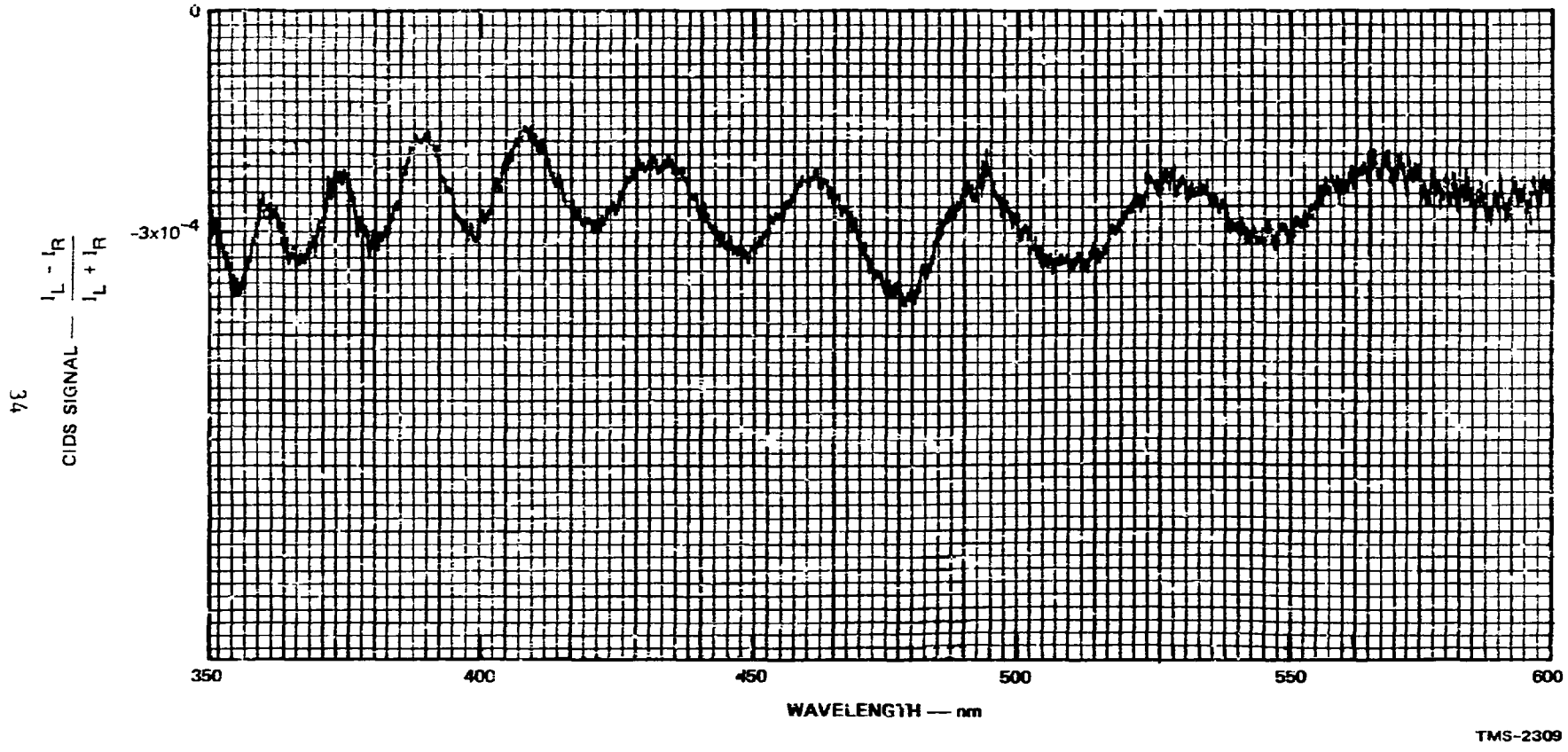

FIGURE 23 168° CIDS ARTIFACT SPECTRUM FROM 2.02-μm POLYVINYL TOLUENE MICROSPHERES

view of remote and local in situ sensing, are the smallest in magnitude and least interesting of the curves. In addition, since the best SNRs obtained with modern DIAL/DISC systems seldom allow a differential measurement much smaller than one part in one thousand, it is unlikely that a pulsed DISC/CIDS lidar system could even detect the 10^{-3} to 10^{-4} CIDS signal from a biological aerosol cloud.

Several methods can be considered for surmounting these problems. One technique is to measure simultaneously several Mueller matrix elements.[12-14] (Recall that CIDS is just one element of the 4x4 Mueller scattering matrix, which has in general 10 independent elements.) By measuring, for example, four or eight elements as a function of wavelength at a fixed scattering angle, one may recover enough information to uniquely specify the scattering material. Unfortunately, for 180° scattering, symmetry considerations show that the Mueller matrix reduces to a very simple form containing only four independent elements, of which CIDS is the only off-diagonal element (see Appendix C). This sharply reduced information content makes it unlikely that differential backscatter will ever allow detection and discrimination of biological aerosols in situ.

An alternative approach to the biological aerosol point-detection problem is simply to collect and preconcentrate aerosol particles from the suspect region. The collected particles may then be suspended in a convenient liquid medium and placed in a cuvette. One may then perform a variety of scattering measurements, either at fixed angle vs. wavelength or at fixed wavelength vs. angle. In this manner, enough information may be obtained to specify the nature of the scattering particles. The success of this approach will depend on whether the Mueller scattering matrix contains enough information to provide a unique scattering signature; however, more laboratory work is necessary to determine this and would require an instrument considerably more sophisticated than the one used in our experiments. For example, an instrument using two or four modulators would allow the simultaneous measurement of four or eight scattering matrix elements.

III PUBLICATIONS AND TECHNICAL REPORTS

Six interim technical reports were prepared during the course of this work on Contract DAAG29-82-K-0126. All are entitled "Infrared Properties of Biological Materials of Interest to the Army." The report numbers, authors, and reporting periods are listed below.

1. Interim Technical Report #1
   Covering the period 30 May 1982 to 31 December 1982

   By: David E. Cooper
   Edward R. Murray

   Published: April 1982

2. Interim Technical Report #2
   Covering the period 1 January 1983 to 30 June 1983

   By: D. E. Cooper
   E. R. Murray
   R. M. Miao

   Published: June 1983

3. Interim Technical Report #3
   Covering the period 30 June 1983 to 31 December 1983

   By: D. E. Cooper

   Published: December 1983

4. Interim Technical Report #4
   Covering the period 1 January 1984 to 30 June 1984

   By: David E. Cooper

   Published: June 1984

5. Interim Technical Report #5
   Covering the period 30 June 1984 to 31 December 1984

   By: David E. Cooper

   Published: December 1984

6. Interim Technical Report #6
Covering the period 1 January 1985 to 30 June 1985
By: David E. Cooper
Published: June 1985

A technical paper discussing the complex refractive indices measurements and the IR DISC measurements is currently in preparation.

A presentation of this work, entitled "Differential Light Scattering from Biological Aerosols," was given by Dr. David E. Cooper at the Third Workshop on the Detection of Biological Agents in Operational Environments, 25-26 April 1984, Raleigh, North Carolina.

IV PARTICIPATING SCIENTIFIC PERSONNEL

Biographies of the following participating personnel are included in this section:

E. Murray

D. Cooper

D. Powell

R. Miao

C. Witham

J. van der Laan

P. Holland

Two consultants, Prof. Milton Kerker of Clarkson College and Prof. Marvin Querry of the University of Missouri, also participated in this project.

EDWARD R. MURRAY

Director
Electro-Optics Systems Laboratory
System Technology Division

SPECIALIZED PROFESSIONAL COMPETENCE

Management of large, multidisciplinary programs; design and construction of infrared lidar systems; remote sensing of gases and aerosols, tunable lasers; infrared optical systems and detectors; molecular spectroscopy; optical properties of aerosols

REPRESENTATIVE RESEARCH ASSIGNMENTS AT SRI (Since 1974)

Project leader for remote sensing of NBC agents
Principal investigator on NSF grant on properties of aerosols
Project supervisor on use of DIAL system for field measurements
Principal investigator on NSF grant for remote measurement of air pollutants
Project leader for CO_2 laser radar to measure properties of smoke and dust at Dugway Proving Ground, Utah
Project leader on application of laser remote sensing to oil and gas exploration
Design, construction, and use of CO_2 laser radar range-resolved measurements of ethylene, ozone, and temperature
Design and testing of DF laser lidar to measure path-integrated concentrations of HC1, CH4, and N_2O

OTHER PROFESSIONAL EXPERIENCE

Research fellow, Stanford University: measure gain and vibrational temperatures in CO_2 lasers; developed model for CO_2 laser
Mechanical engineer, Harry Diamond Laboratories: design and testing of batteries and high-pressure gas guns
Research fellow, George Washington University: analysis of effect of radiation on flow around a hypersonic reentry vehicle

ACADEMIC BACKGROUND

B.S.M.E. (1967) and M.S.M.E. (1969) specializing in fluid mechanics, George Washington University; Ph.D. in laser physics (with distinction, 1974), Stanford University

PUBLICATIONS AND PRESENTATIONS

Ten professional journal articles; guest lecturer, Stanford University; numerous presentations at professional symposia; numerous SRI reports

PROFESSIONAL ASSOCIATIONS AND HONORS

Sigma Xi, Tau Beta Pi, Optical Society of America; Optical Society of Northern California

DAVID E. COOPER

Senior Research Physicist
Electro-Optics Systems Laboratory
System Technology Division

SPECIALIZED PROFESSIONAL COMPETENCE

Applied experimental physics; visible, ultraviolet, and infrared lasers; picosecond spectroscopy, nonlinear optics and light scattering; remote sensing of the atmosphere using lidar and passive infrared systems; frequency modulation spectroscopy

REPRESENTATIVE RESEARCH ASSIGNMENTS AT SRI (Since 1982)

Development of infrared frequency modulation spectroscopy for ultra sensitive detection of gaseous molecular species using tunable and fixed frequency laser sources

Infrared properties of and light scattering from biological materials and natural aerosols

Circular-intensity differential scattering (CIDS) from suspensions and aerosols of biological materials

Remote detection of nuclear, biological, and chemical contamination in the atmosphere

Passive infrared remote sensing technology

Point detection of atmospheric trace gases using tunable diode laser derivative spectroscopy

High PRF CO_2 laser heterodyne lidar systems

OTHER PROFESSIONAL EXPERIENCE

Technical Staff Member, Los Alamos National Laboratory: development of advanced optical characterization techniques in the visible and infrared for laser fusion targets; phase modulation interferometry; light scattering by small glass and metal shells; ellipsometry and Fourier transform optics

Graduate Research Assistant, MIT: construction of passively mode locked CW dye laser; studies of molecular orientational dynamics in liquids; magentism in solids and low temperature physics

ACADEMIC BACKGROUND

B.S. in Physics (magna cum laude, 1974), University of California, Los Angeles, CA

Ph.D. in Physics (1980), Massachussetts Institute of Technology, Cambridge, MA

PROFESSIONAL ASSOCIATIONS AND HONORS

American Physical Society; Optical Society of America; Society of Photo-Optical Instrumentation Engineers; Karl Taylor Compton Graduate Fellow (MIT); Sigma Pi Sigma

December 1985

PUBLICATIONS OF DR. DAVID E. COOPER

Cooper, D. E., and T. F. Gallagher, "Double Frequency Modulation Spectroscopy: High Modulation Frequency with Low-Bandwidth Detectors," Applied Optics, Vol. 24, p. 1327, 1985

Cooper, D. E., and T. F. Gallagher, "Frequency Modulation Spectroscopy with a CO_2 Laser: Results and Implications for Ultrasensitive Point Monitoring of the Atmosphere," Applied Optics, Vol. 24, p. 710, 1985

Hawley, J. G., D. D. Powell, and D. E. Cooper, "Absorption Coefficient of Ammonia for Laser Remote Sensing of Atmospheric Trace Quantities," paper WC28 in Optical Remote Sensing of the Atmosphere, Technical Digest, January 15-18, 1985, Incline Village, Nevada

Cooper, D. E., and T. F. Gallagher, "Frequency Modulation Spectroscopy with a Multimode Laser," Optics Letters, Vol. 9, p. 451, 1984

Cooper, D. E., and E. R. Murray, "Differential Light Scattering from Biological Aerosols," presented at the Third ARO Biodetection Workshop, Raleigh, North Carolina, April 25-26, 1984

Hawley, J. G., D. D. Powell, T. F. Gallagher, R. E. Warren, and D. E. Cooper, "Remote and In-Situ Detection of Atmospheric Trace Gases," EPRI Contract RP-1370, Final Report, November 1983

Cooper, D. E. Dau-Sing Wang, and M. Kerker, "Scattering of Light by Laser Fusion Targets with Small Defects," Applied Optics, Vol. 22, p. 83, 1983

Cooper, D. E., "A Phase Modulation Interferometer for ICF Target Characterization," J. Vac. Sci. Technol. 20(4), p. 1075, 1982

Cooper, D. E. and J. D. Litster, "Molecular Orientation Dynamics in Gels and Critical Mixtures," in "Picosecond Phenomena II," R. Hochstrasser, W. Kaiser and C. V. Shank, editors, Springer-Verlag, Berlin, Heidelberg, New York, 1980

DIANE D. POWELL

Research Engineer
Electro-Optics Systems Laboratory
System Technology Division

SPECIALIZED PROFESSIONAL COMPETENCE

Remote sensing of gases, aerosols, and surface contamination using Differential Absorption Lidar (DIAL) and Differential Scatter Lidar (DISC). Fourier Transform Infrared (FTIR) Spectroscopy.

REPRESENTATIVE RESEARCH ASSIGNMENTS AT SRI (Since 1979)

CO_2 laser reflectance measurements and FTIR measurements of diffuse reflectance from surfaces

Remote measurement of backscattered signatures from aerosols

CO_2 lidar studies near 10 um for ambient temperature determination

Remote measurement calibrated concentrations of DMMP with CO_2 lidar

Remote measurement of NH_3 absorption coefficient at 1084 cm^{-1} with CO_2 lidar

Hydrocarbon concentration measurements with a Nd:YAG-pumped dye laser and nonlinear mixing in $LiNbO_3$

CO_2 DISC measurements of SF-96 aerosol backscattered radiation

CO_2 DISC measurements of backscatter from dusts

OTHER PROFESSIONAL EXPERIENCE

Operation and characterization of Fourier transform spectrometer for remote sensing of pollutants in the infrared region for Environmental Protection Agency, Research Triangle Park, North Carolina

Operation of spectrometer for Raman-scattering study of Cd-doped Cu_2O at Kansas State University

ACADEMIC BACKGROUND

M.S. Physics (1976), B.S. Astronomy (1974), University of Oklahoma

PUBLICATIONS AND PRESENTATIONS

Author and co-author of several client-private publications for SRI International clients

Co-author "Absorption Coefficient of Ammonia for Laser Remote Sensing of Atmospheric Trace Quantities" to be published.

Co-author "Measurement of Average Atmospheric Temperature Using a CO_2 Laser Radar," Applied Optics (June 1980)

Author "A New Method for Measuring the Normal Fluid Density of Liquid ^4He," Thesis, University of Oklahoma (1976)

Co-author "Raman-Scattering Study of Ion-Implantation-Produced Damage in Cu_2O" Phys. Rev. B (July, 1975)

PROFESSIONAL ASSOCIATIONS

Optical Society of America, Sigma Pi Sigma (National Physics Honor Society), Toastmasters International

RAYMOND M. MIAO

Senior Biochemist, Cell Biologist
Molecular Biochemistry Program
Biomedical Research Department
Life Sciences Division

SPECIALIZED PROFESSIONAL COMPETENCE

Tissue culture with emphasis on mutagenization, isolation, and characterization of cells, cell fusion, and cell biology (regulation of differentiation and growth); biochemistry and genetics of animal cells (hematopoietic cells and epidermal/epithelial cells) with emphasis on the role of plasma membrane components and protein kinases on cell differentiation and growth; DNA-mediated transformation and chromosome-mediated gene transfer in animal cells in culture; biochemistry, immunology, and genetics of oncogenic viruses (DNA and RNA viruses); new drug development with emphasis on developing rapid in vivo and in vitro assay systems; in vivo and in vitro chemical and viral carcinogenesis and tumor promotion; nucleic acid biochemistry (integration, recombination, and replication); bacterial genetics; animal cell-virus interactions; mammalian chromosome structure-function relationships; molecular aspects of eukaryotic and viral gene expression; bacterial transformation; genetics and biochemistry of Treponema pallidum

INITIATED FOLLOWING RESEARCH PROGRAMS AT SRI

Development of in vitro transformation assays for chemical carcinogens
Development of mammalian cell mutagenesis assay for chemical carcinogens
Analysis of the in vitro metabolic activation of procarcinogens
Studies on the regulation of erythroid and leukemic cell differentiation
Development of procedures for the isolation and cultivation of primary epidermal basal cells (stem cell of skin)
Genetic studies of proerythroid cells using cell fusion techniques
Studies on the mechanism of action of tumor promoters in vivo and in vitro
Studies on the relationship between tumor progression and immune system functions in vivo
Development and in vivo and in vitro evaluation of chemopreventive anticancer drugs
Development of drugs which induce cellular differentiation
Development of new immunomodulatory drugs
Establish plant cell biotechnology program (market analysis, product development, initiate and supervise cell culture laboratory)
Determination of the genetic relationships between T. pallidum and other pathogenic and nonpathogenic treponemes
Biochemical and biophysical analyses of unscheduled DNA synthesis in tissue culture cells
Determination of nucleic acid sequence homology
Development of procedures for labeling DNA with ^{125}I to high specific activity

Tissue culture including establishment of primary cultures from mouse organs, hamster embryos, and chemically and virally induced rat tumors
Develop molecular electronic devices (biosensors, biocircuits, and ultimately biocomputers)

OTHER PROFESSIONAL EXPERIENCE

Research associate, Department of Microbiology, Upstate Medical Center, Syracuse, NY; immunological, biochemical, and biological techniques relating to avian oncornaviruses and human papovaviruses
Postdoctoral fellow, Wistar Institute, Philadelphia, PA; studies on the biochemistry and genetics of RNA tumor viruses including the enzymology of viral-associated, RNA-dependent DNA polymerase; development of a system for the isolation and uptake of functional metaphase chromosomes in tissue culture cells (chromosome transfer)

ACADEMIC BACKGROUND

A.B. in chemistry (1965), Queens College, CUNY; Ph.D. in biochemistry (1971), Duke University

PUBLICATIONS

Author or coauthor of 12 technical publications

August 1985

CLYDE L. WITHAM

Manager
Fine Particle Technology Program
Chemical Engineering Laboratory
Physical Sciences Division

SPECIALIZED PROFESSIONAL COMPETENCE
Fine particle technology; aerosol generation technology; air pollution control; equipment design

REPRESENTATIVE RESEARCH ASSIGNMENTS AT SRI (since 1973)
Development of aerosol generation techniques for fine particle research
SO_x, NO_x scrubber studies
Research on mechanisms of fine particulate removal in wet scrubbers
Inhalation toxicology of numerous gaseous and aerosol materials
Design of inhalation exposure facilities
Biological aerosol detection techniques, point and remote sensing
Air pollution studies in the steel and pesticide manufacturing industries
Air pollution studies on agricultural-refuse-fired boilers
Environmental emissions from the mining and minerals industry
Development of methods for aerosol particle size measurement
Development and evaluation of methods of fugitive emissions measurement
Industrial hygiene surveys in the pesticide and aluminum industries
Assessment of industrial hygiene and dust generation problems in the solid waste recovery industry
Production of novel screening smokes
Powder feeding and dispersion techniques
Comminution and energy consumption
Particulate collection characteristics of negative ion generators
Aerosol drug delivery
Air purifying respirator effectiveness

OTHER PROFESSIONAL EXPERIENCE
Kennecott-Copper Corporation and Brigham Young University: monitoring of SO_x stack emissions from copper smelters
Thermochemical Research Center, Brigham Young University: study of thermodynamic properties of multicomponent, two-phase systems

ACADEMIC BACKGROUND
B.S. in chemical engineering (1973), Brigham Young University;
M.S. in environmental engineering (1977), Stanford University

PUBLICATIONS
Author or coauthor of more than twenty-five papers, reports, and presentations on aerosols, aerosol generation and monitoring, biological aerosols, powder dispersion, and air pollution control.

PROFESSIONAL ASSOCIATIONS AND HONORS
American Institute of Chemical Engineers; American Chemical Society, American Association of Aerosol Research; Tau Beta Pi

LANGUAGE PROFICIENCY
Spanish

JAN VAN DER LAAN

Senior Research Engineer
Electro-Optics Systems Laboratory
System Technology Division

SPECIALIZED PROFESSIONAL COMPETENCE

Fiber optic communication techniques; design and construction of high-energy infrared (IR) laser and dye laser systems for laboratory and laser radar (lidar) applications, ionosphere sounder systems; radio communications; radar systems

REPRESENTATIVE RESEARCH ASSIGNMENTS AT SRI (Since 1964)

Project leader for remote sensing techniques for chemical agent detection
Project leader for CO_2 lidar measurements of IR properties of battlefield dust and smoke
Project leader for IR lidar design and construction
Task leader for design of three-wavelength lidar control, receiver, and auto tracking system
Principal investigator on optical TDR system IR&D development program for fiber optic waveguide
Task leader on several lidar development programs for remote measurement of gaseous pollutants and atmospheric constituents
Task leader for coaxial dye laser development program for lidar applications
Technical consultant to the Military R&D Center of Thailand
Several electromagnetic pulse (EMP) data collection, interpretation, and susceptibility programs
Several ionospheric and communications research programs

OTHER PROFESSIONAL EXPERIENCE

Vitro Services; supervision of field personnel during high-altitude nuclear test series; ionospheric research program in New Jersey; communications evaluation program in South Vietnam
U.S. Army; radar and computer maintenance

ACADEMIC BACKGROUND

U.S. Santa Barbara fiber optic communications course; schooling in radar and computer systems (1958), U.S. Army; attended University of Florida

PRESENTATIONS AND PUBLICATIONS

Optical Fiber Technology presentation at Electro-78 Professional Symposium (May 1978); coauthor of 6 professional journal articles pertaining to lidar and remote sensing; author or coauthor of 3 professional journal articles pertaining to ionospherics and radio propagation; author or coauthor of numerous SRI reports and classified reports

PROFESSIONAL ASSOCIATIONS

FCC First Class Radiotelephone with Ship Radar endorsement; Optical Society of America

September 1984

PETER L. HOLLAND

Research Engineer
Electro-Optics Systems Laboratory
System Technology Division

SPECIALIZED PROFESSIONAL COMPETENCE
Remote sensing of gases; construction of lidar systems; microprocessor applications; software and hardware development of deliverable systems

REPRESENTATIVE RESEARCH ASSIGNMENTS AT SRI (Since 1982)
Analysis of infrared laser radar data for chemical agent detection
Field operation of an infrared laser radar measuring chemical agent simulants
Design and implementation of a real-time data acquisition, processing, and display system for an infrared laser radar
Use of an infrared spectrophotometer to analyze spectral reflectance modifications of surfaces contaminated with a chemical agent simulant
Field operation of an ultraviolet laser radar measuring air pollution
CO_2 DISC measurements of biological aerosols

ACADEMIC BACKGROUND
B.A. in Physics, University of California, Berkeley (1982)
Graduate work in Applied Physics, Stanford University

PUBLICATIONS
Coauthor of annual SRI report to CRDC; coauthor of SRI report on IR DISC studies

PROFESSIONAL ASSOCIATIONS
Optical Society of America

V BIBLIOGRAPHY

1. Mudd, H. T., C. H. Kruger, and E. R. Murray, "Measurement of IR Laser Backscatter Spectra from Sulfuric Acid and Ammonium Sulfate Aerosols," Applied Optics, 21, 1146, 1982.

2. Atkins, P. W., and L. D. Barron, "Rayleigh Scattering of Polarized Photons by Molecules," Mol. Phys., 16, 453, 1969.

3. Bustamante, C., M. F. Maestre, and I. Tinoco, "Circular-Intensity Differential Scattering of Light by Helical Structures--I: Theory," J. Chem. Phys., 73(9), 4273, 1980.

4. Bustamante, C., M. F. Maestre, and I. Tinoco, "Circular-Intensity Differential Scattering of Light by Helical Structures--II: Applications," J. Chem. Phys., 73(12), 6046, 1980.

5. Bustamante, C., I. Tinoco, and M. F. Maestre, "Circular-Intensity Differential Scattering of Light by Helical Structures--III: A General Polarizability Tensor and Anomalous Scattering," J. Chem. Phys., 74(9), 4839, 1981.

6. Bustamante, I. Tinoco, and M. F. Maestre, "Circular Intensity Differential Scattering of Light--IV: Randomly Oriented Species," J. Chem. Phys.,76(7), 3440, 1982.

7. Salzman, G. C., J. K. Griffith, and C. T. Gregg, "Rapid Identification of Microorganisms by Circular-Intensity Differential Scattering," Appl. Environ. Micro., 44, 1081, 1982.

8. Salzman, G. C., and C. T. Gregg, "Current and Experimental Methods of Rapid Microbial Identification," Biotechnology, March 1984.

9. Jasperson, S. N., and S. E. Schnatterly, Rev. Sci. Inst., 40, 761, (1969); J. C. Kemp, J. Opt. Soc. Am., 59, 950, 1969.

10. Shurcliff, W. A., Polarized Light, Harvard University Press, Cambridge, Massachusetts, 1962.

11. van de Hulst, H. C., Light Scattering by Small Particles, Dover Publications, Inc., New York, 1957.

12. Bickel, W. S., J. F. Davidson, D. R. Huffman, and R. Kilkson, "Application of Polarization Effects in Light Scattering: A New Biophysical Tool," Proc. Nat. Acad. Sci., USA, 73, 486, 1976.

13. Hunt, A. J., and D. R. Huffman, "A New Polarization-Modulated Light Scattering Instrument," Rev. Sci. Inst., 44, 1753, 1973.

14. Thompson, R. C., J. R. Bottiger, and E. S. Fry, "Measurement of Polarized Light Interactions Via the Mueller Matrix," Applied Optics, 19, 1323, 1980.

Appendix A

SENSITIVITY LIMITS OF IR DISC FOR BIOLOGICAL AEROSOL DETECTION

An estimate of the sensitivity of IR DISC to a biological aerosol cloud can be obtained from the lidar equation as follows. Imagine the situation depicted in Figure A-1. An infrared lidar system transmits two light pulses at wavelengths λ_1 and λ_2 and measures the backscattered return from a biological aerosol cloud of depth ΔR, located at range R. The lidar equation gives the power returned from the cloud at wavelength λ as

$$P_r(\lambda,\Delta R) = k(\Delta R)\,\frac{A_r}{R^2}\,P_t(\lambda)\beta_\pi(R,\lambda)e^{-2\int_0^R k_{ext}(r,\lambda)\,dr}, \qquad \text{(A-1)}$$

where

k = overall optical system efficiency factor
A_r = aperture of receiving optics
P_t = transmitted power at wavelength λ
$\beta_\pi(R,\lambda)$ = total aerosol backscattering coefficient
$k_{ext}(r,\lambda)$ = atmospheric extinction coefficient.

We now define our signal, S, as the difference between the power normalized returns at wavelengths λ_1 and λ_2 divided by their sum:

$$S = \frac{\dfrac{P_r(R,\lambda_1)}{P_t(\lambda_1)} - \dfrac{P_r(R,\lambda_2)}{P_t(\lambda_2)}}{\dfrac{P_r(R,\lambda_1)}{P_t(\lambda_1)} + \dfrac{P_r(R,\lambda_2)}{P_t(\lambda_2)}}. \qquad \text{(A-2)}$$

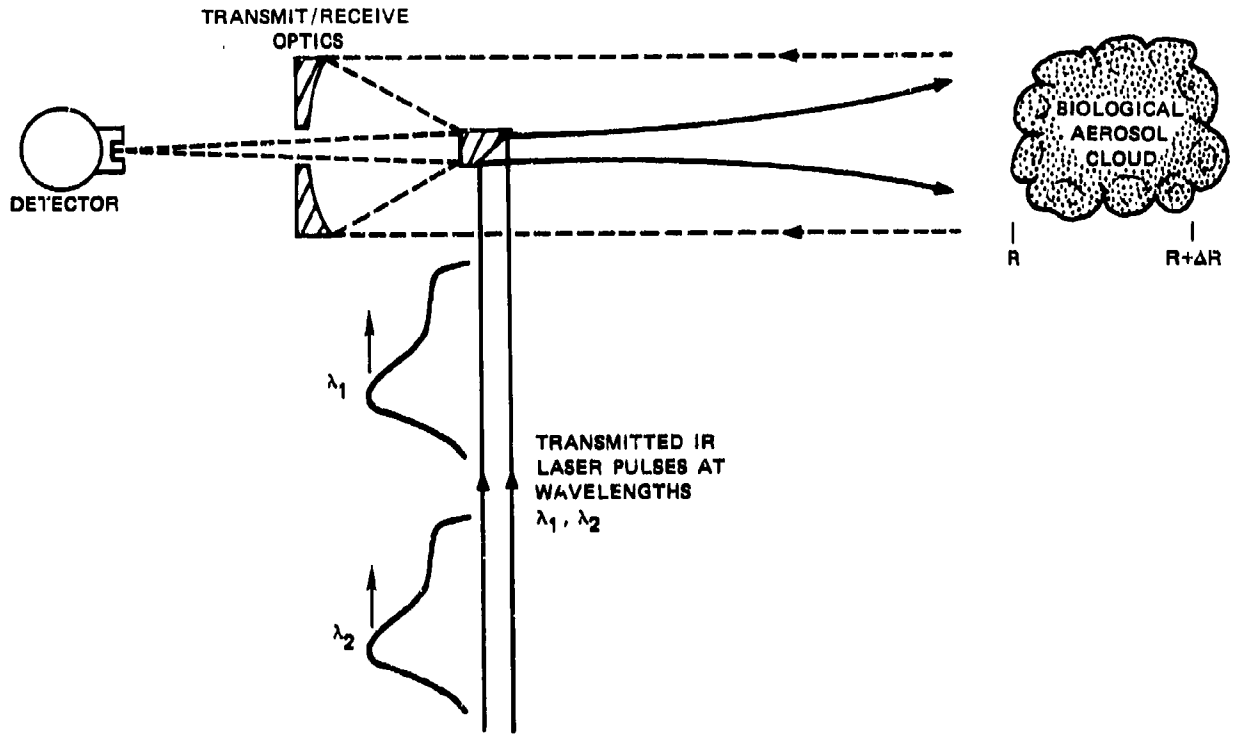

FIGURE A-1 IR DISC LIDAR SYSTEM

By use of the lidar equation, this signal reduces to

$$S = \frac{\beta_\pi(R,\lambda_1) - \beta_\pi(R,\lambda_2)\, e^{-2\int_0^R \Delta k_{ext}(r)dr}}{\beta_\pi(R,\lambda_1) + \beta_\pi(R,\lambda_2)\, e^{-2\int_0^R \Delta k_{ext}(r)dr}}, \qquad (A-3)$$

where

$$\Delta k_{ext}(r) = k_{ext}(r,\lambda_1) - k_{ext}(r,\lambda_2).$$

We will now assume that the atomspheric extinction can be ignored, i.e., $\Delta k_{ext} \approx 0$. This is, in general, a clearly invalid assumption;

however, ignoring it in our expression for S yields the maximum differential signal that we can expect from our aerosol cloud. Hence, the sensitivity estimate obtained using this assumption is a best-case estimate. With $\Delta k_{ext}(r) = 0$, our signal becomes simply

$$S = \frac{\beta_\pi(R,\lambda_1) - \beta_\pi(R,\lambda_2)}{\beta_\pi(R,\lambda_1) + \beta_\pi(R,\lambda_2)} \quad . \tag{A-4}$$

Now the total backscattering coefficient, β_π, can be separated into a sum of two terms: the first term is the backscattering contribution from the target biological aerosol cloud, and the second term is the contribution from the atmospheric background aerosol. Explicitly, we write

$$\beta_\pi(R,\lambda) = N(R)\sigma_\pi(\lambda) + \beta_\pi^{bak}(R,\lambda) \quad , \tag{A-5}$$

where

$N(R)$ = biological aerosol cloud number density

$\sigma_\pi(\lambda)$ = average backscattering cross section of the biological aerosol particles

$\beta_\pi^{bak}(R,\lambda)$ = atmospheric aerosol background contribution.

This gives our final result for the DISC signal as

$$S = \frac{N(R)\,\Delta\sigma_\pi + \Delta\beta_\pi^{bak}(R)}{2N(R)\,\bar{\sigma}_\pi + 2\bar{\beta}_\pi^{bak}(R)} \quad , \tag{A-6}$$

where

$$\Delta\sigma_\pi = \sigma_\pi(\lambda_1) - \sigma_\pi(\lambda_2)$$

$$\Delta\beta_\pi^{bak}(R) = \beta_\pi^{bak}(R,\lambda_1) - \beta_\pi^{bak}(R,\lambda_2)$$

$$\bar{\sigma}_\pi = \tfrac{1}{2}[\sigma_\pi(\lambda_1) + \sigma_\pi(\lambda_2)]$$

$$\bar{\beta}_\pi^{bak}(R) = \tfrac{1}{2}[\beta_\pi^{bak}(R,\lambda_1) + \beta_\pi^{bak}(R,\lambda_2)] \quad .$$

The complex refractive index data and aerosol backscattering data obtained at SRI for biological materials show that the backscattering cross section for biological aerosols varies quite slowly with wavelength in the 8- to 12-μm atmospheric window transmission region. Furthermore, obtaining a significant backscattering differential, $\Delta\sigma_\pi$, requires a wavelength differential of several microns. However, over an interval of $\Delta\lambda \approx 1\mu m$, the atmospheric volume backscattering coefficient usually changes significantly, i.e., $\Delta\beta_\pi^{bck} \approx 10^{-8}\ m^{-1}sr^{-1}$. For comparison, based on SRI's data, a 3-μm MMD aerosol of B. subtilis spores with a density of 1 particle/cc would give a maximum differential backscatter of $\Delta\sigma_\pi \approx 10^{-10}\ m^{-1}sr^{-1}$ for a wavelength differential of 1 μm in the 8- to 12-μm region. Hence, the biological aerosol cloud and atmospheric background aerosol differential backscatter terms are comparable (i.e., $N\Delta\sigma_\pi \approx \Delta\beta_\pi^{bck}$) only for $N \approx 100$ particles/cc. This best-case detection limit far exceeds the Army's desired detection sensitivity limits of 5 to 10 particles/liter (0.05 to 0.10 particles/cc) for biological aerosol clouds.

Appendix B

ORIGIN OF CIDS ARTIFACT SIGNALS

An understanding of the cause of the artifact signals in our experiments follows from a detailed analysis of the Stokes vector of the light beam as it propagates from the source through the modulator and scattering suspension to the photodetector. The effect of each element in the optical path on the polarization state of the light beam can be represented by the 4x4 Mueller matrix of the optical element operating on the four-component Stokes vector.[10] If we consider the optical configuration shown in Figure 12 with the quartz cuvette assumed to contain an optically inactive suspension of polystyrene microspheres, then the Stokes vector of the detected scattered light is given by matrix multiplication as

$$\begin{vmatrix} I \\ Q \\ U \\ V \end{vmatrix} = \begin{vmatrix} \tfrac{1}{2}(m_2 + m_1) & \tfrac{1}{2}(m_2 - m_1) & 0 & 0 \\ \tfrac{1}{2}(m_2 - m_1) & \tfrac{1}{2}(m_2 + m_1) & 0 & 0 \\ 0 & 0 & S_{21} & -D_{21} \\ 0 & 0 & D_{21} & S_{21} \end{vmatrix} \begin{vmatrix} 1 & 0 & 0 & 0 \\ 0 & 1 & 0 & 0 \\ 0 & 0 & \cos\delta & \sin\delta \\ 0 & 0 & -\sin\delta & \cos\delta \end{vmatrix} \begin{vmatrix} 1 \\ 0 \\ 1 \\ 0 \end{vmatrix} I_o$$

$$= \begin{vmatrix} \tfrac{1}{2}(m_2 + m_1) \\ \tfrac{1}{2}(m_2 - m_1) \\ S_{21}\cos\delta + D_{21}\sin\delta \\ D_{21}\cos\delta - S_{21}\sin\delta \end{vmatrix} I_o \qquad \text{(B-1)}$$

The [1,0,1,0] column vector is the Stokes vector for light linearly polarized at +45° and represents the output of the Glan-Thompson prism polarizer. The first Mueller matrix represents the effect of the

photoelastic polarization modulator with its induced optic axis oriented at 0°, and $S = A \sin \omega t$, where ω is the modulation frequency ($\omega/2\pi$ = 50 kHz). The second Mueller matrix is essentially the Mie scattering matrix for spheres taken from van de Hulst,[11] who gives detailed expressions for the coefficients m_1, m_2, S_{21}, and D_{21}, all of which depend on scattering angle. The essential result of this calculation is that the intensity of the detected light is simply $I = \frac{1}{2}(m_1 + m_2)$, which is clearly not affected by the polarization modulation and therefore contains no time-varying (ac) components.

In our scattering experiments on suspensions of polystyrene microspheres using the above configuration, we routinely observed first-harmonic (ω) and second-harmonic (2ω) components on the scattered light. Hence, the above treatment is an incomplete description of the apparatus because some additional polarization effects are not included. The essential effect left out of the above calculation is the linear birefringence of the focusing lenses and the cuvette windows. The Mueller matrix of a general elliptical retarder of any retardance, ϕ, and azimuthal angle, δ, can be written in the form

$$\begin{vmatrix} 1 & 0 & 0 & 0 \\ 0 & a_1 & a_2 & a_3 \\ 0 & b_1 & b_2 & b_3 \\ 0 & c_1 & c_2 & c_3 \end{vmatrix} . \qquad \text{(B-2)}$$

The detailed relationships between the matrix elements a_1, a_2, a_3,..... and ϕ and δ are given by Shurcliff.[10] If such a matrix is inserted before and after the scattering matrix in Eq. (B-1), one obtains

$$\begin{vmatrix} I \\ Q \\ U \\ V \end{vmatrix} = \begin{vmatrix} 1 & 0 & 0 & 0 \\ 0 & r_1 & r_2 & r_3 \\ 0 & s_1 & s_2 & s_3 \\ 0 & t_1 & t_2 & t_3 \end{vmatrix} \begin{vmatrix} \frac{1}{2}(m_1+m_2) & \frac{1}{2}(m_2-m_1) & 0 & 0 \\ \frac{1}{2}(m_1-m_2) & \frac{1}{2}(m_2+m_1) & 0 & 0 \\ 0 & 0 & S_{21} & -D_{21} \\ 0 & 0 & D_{21} & S_{21} \end{vmatrix} \begin{vmatrix} 1 & 0 & 0 & 0 \\ 0 & a_1 & a_2 & a_3 \\ 0 & b_1 & b_2 & b_3 \\ 0 & c_1 & c_2 & c_3 \end{vmatrix} \begin{vmatrix} 1 \\ 0 \\ \cos\delta \\ -\sin\delta \end{vmatrix} I_o$$

$$= \begin{vmatrix} 1 & 0 & 0 & 0 \\ 0 & r_1 & r_2 & r_3 \\ 0 & s_1 & s_2 & s_3 \\ 0 & t_1 & t_2 & t_3 \end{vmatrix} \begin{vmatrix} \tfrac{1}{2}(m_1+m_2) + \tfrac{1}{2}(m_2-m_1)(a_2\cos\delta - a_3\sin\delta) \\ \tfrac{1}{2}(m_2-m_1) + \tfrac{1}{2}(m_2+m_1)(a_2\cos\delta - a_3\sin\delta) \\ S_{21}(b_2\cos\delta - b_3\sin\delta) - D_{21}(c_2\cos\delta - c_3\sin\delta) \\ D_{21}(b_2\cos\delta - b_3\sin\delta) + S_{21}(c_2\cos\delta - c_3\sin\delta) \end{vmatrix} I_o$$

(B-3)

From this, we observe that it is only the birefringence of the focusing lens and cuvette entrance window, represented collectively by the matrix (B-2), that give rise to ac components in the scattered intensity, $I = I_o[\tfrac{1}{2}(m_2+m_1) + \tfrac{1}{2}(m_2-m_1)(a_2\cos\delta - a_3\sin\delta)]$. Birefringence in the exit windows of the cuvette or in the collection lens does not give rise to artifact signals. Using the Bessel function expansions for cos δ and sin δ,

$$\cos\delta = \cos(A\sin\omega t) = J_o(A) + 2\sum_{1}^{\infty} J_{2n}(A)\cos 2n\omega t$$

$$\sin\delta = \sin(A\sin\omega t) = 2\sum_{0}^{\infty} J_{2n+1}(A)\sin[(2n+1)\omega t] \quad . \tag{B-4}$$

We conclude that the intensity of light scattered from a suspension of spheres in the presence of linear birefringence will contain ac components at both the even and odd harmonics of the modulation frequency. Furthermore, an analysis of the coefficients a_2 and a_3 given by Shurcliff[10] shows that $a_2 \approx \phi^2$ and $a_3 \approx \phi$. Hence, the odd harmonic components are expected to be stronger than the even harmonic components since $\phi << 1$. This is in fact what we observe in our measurements. In addition, van de Hulst[11] shows that in the Rayleigh limit (i.e., $\lambda >>$ particle circumference), the factor $\tfrac{1}{2}(m_2-m_1)$ simply reduces to $\sin^2\theta$, which is a maximum at $\theta = \pm 90°$ and vanishes at $\theta = 0°$ or 180°. This explains why our artifact signals are smaller for backscattering than for 90° scattering ($\sin^2 90° = 1$, $\sin^2 168° \approx 4\times10^{-2}$). Also, in the Rayleigh limit, the shape of the artifact curves should not change as θ varies from 90° to 180°; only the overall magnitude should change as dictated by the $\sin^2\theta$ factor.

Appendix C

CIDS FROM SUSPENSIONS OF BIOLOGICAL MICROORGANISMS

The Stokes vector treatment of our light-scattering apparatus, discussed in Appendix B, can easily be extended to cover the case in which the scattering suspension consists of biological microorganisms. However, additional complexity is introduced because the scattering Mueller matrix now contains more non-zero elements. According to van de Hulst,[11] the most general form of the Mueller matrix for scattering at any arbitrary angle has ten independent parameters and is given by

$$\begin{vmatrix} \alpha_1 & \beta_1 & \beta_3 & \beta_5 \\ \beta_1 & \alpha_2 & \beta_4 & \beta_6 \\ -\beta_3 & -\beta_4 & \alpha_3 & \beta_2 \\ \beta_5 & \beta_6 & -\beta_2 & \beta_4 \end{vmatrix} \quad . \tag{C-1}$$

Substitution of this scattering matrix for the one used in Eq. (B-3) of Appendix B gives, for the scattered intensity,

$$I = [\alpha_1 + (\beta_1 a_2 + \beta_3 b_3 + \beta_5 c_2) \cos \delta - (\beta_1 a_3 + \beta_3 b_3 + \beta_5 c_3) \sin \delta] I_0 \quad . \tag{C-2}$$

From the expressions given in Shurcliff, it can be shown that $a_3 \approx b_3 \approx \phi$ and $c_3 \approx 1$. Since the residual linear birefringence, ϕ, is small, we expect $c_3 >> a_3$ or b_3 so that we might expect the $\beta_5 c_3$ term in the coefficient for $\sin \delta$ to be the dominant term. This is in fact the term of interest since it can easily be shown that it is the

β_3 element in the Mueller matrix (C-1) that gives rise to differential scattering of left and right circularly polarized light. The remaining terms, $\beta_1 a_3$ and $\beta_3 b_3$, result from linear birefringence in the focusing optics and cuvette entrance window. Hence, in the presence of this linear birefringence, the measured signal at the fundamental of the modulation frequency, ω, is a combination of CIDS and linear birefringence. Whether CIDS or linear birefringence dominates the signal depends on the magnitude of the birefringence, ϕ, and the relative magnitude of the matrix elements β_1, β_3, and β_5.

In the case of backscattering, a great simplification in this analysis results from symmetry arguments, as discussed by van de Hulst. If the suspension of scattering particles exhibits rotational symmetry (i.e., the distribution of the particles in all possible orientations does not change if the entire suspension is rotated about the scattering axis), then the Mueller matrix for backscatter reduces to the simple form

$$\begin{vmatrix} \alpha_1 & 0 & 0 & \beta_5 \\ 0 & \alpha_2 & 0 & 0 \\ 0 & 0 & -\alpha_2 & 0 \\ \beta_5 & 0 & 0 & \alpha_4 \end{vmatrix} \quad . \tag{C-3}$$

Using this scattering matrix in Eq. (B-3) gives, for the scattered intensity,

$$I = \left[\alpha_1 + \beta_3 c_2 \cos\delta - \beta_5 c_3 \sin\delta\right] I_o \quad . \tag{C-4}$$

Hence, for backscattering ($\theta = 180°$), there is no significant contamination from linear birefringence. In addition, one would expect that for near-backscattering angles ($\theta \sim 170°$), the linear birefringence artifact should be small. This is one advantage that CIDS backscatter measurements have over CIDS measurements at other angles.

In our experiment, the component of the intensity that oscillates at the modulation frequency, ω, is divided by the dc component to give the signal, S. From (C-4) and (B-4) the result is

$$S = \frac{-2J_1(A)\ \beta_s c_3 \sin \omega t}{\alpha_1} \quad . \tag{C-5}$$

Using the Stokes vectors for left and right circularly polarized light, [1,0,0,1] and [1,0,0,-1], respectively, and the scattering matrix, Eq. (C-3), it is easily shown that

$$\frac{\beta_s}{\alpha_1} = \frac{I_L(\theta) - I_R(\theta)}{I_L(\theta) + I_R(\theta)} = \frac{\Delta I}{2\bar{I}} \tag{C-6}$$

is the CIDS signal defined in Eq. (3) of the main report.

An estimate of the minimum detectable differential signal can be obtained by comparing the detector photocurrent power at ω to the shot noise power. From Eqs. (C-4) and (B-4), the photocurrent component at ω is given by

$$i_s = -g \frac{e\eta}{h\nu} I_o \beta_s c_3\ 2J_1(A) \sin \omega t \quad , \tag{C-7}$$

where

g = photodetector gain

η = photodetector quantum efficiency

ν = light frequency

e and h = fundamental constants.

The mean-square signal power is therefore

$$\langle i_s^2 \rangle = 2g^2 \left(\frac{e\eta}{h\nu} I_o \right)^2 J_1^2(A)\ (\beta_s c_3)^2 \quad . \tag{C-8}$$

The mean-square shot noise power is given by

$$\langle i_{sn}^2 \rangle = 2g^2 e^2 \eta \left(\frac{I_o}{h\nu} \right) \Delta f \, \alpha_1 \quad , \tag{C-9}$$

where Δf is the detection bandwidth. Hence, the SNR is given by

$$\text{SNR} = \frac{\langle i_s^2 \rangle}{\langle i_{sn}^2 \rangle} = \frac{\eta I_o J_1^2(A) \beta_s^2 \sigma_s^2}{h\nu \cdot \Delta f \cdot \alpha_1} = \frac{\eta I_o J_1^2(A) (\Delta I)^2 \sigma_s^2 \alpha_1}{4 \Delta f \bar{I}^2 h\nu} \quad , \tag{C-10}$$

where the last step follows from Eq. (C-6). Defining the minimum detectable CIDS signal as that signal giving a SNR of unity, Eq. (C-10) can be inverted to give

$$\frac{\Delta I}{2\bar{I}}_{\min} = \left[\frac{h\nu \cdot \Delta f}{\eta I_o J_1^2(A) \sigma_s^2 \alpha_1} \right]^{1/2} \tag{C-11}$$

In our experiment, typical values for these parameters are:

$$\eta \approx 0.25$$
$$\nu = 6.7 \times 10^{14} \text{ Hz}$$
$$\Delta f = 1 \text{ Hz},$$
$$\sigma_s^2 \alpha_1 I_o \approx 10^{-9} \text{ W}$$
$$J_1(A) = 0.58.$$

Inserting these in Eq. (C-11) gives $[\Delta I/2\bar{I}]_{\min} \approx 7.25 \times 10^{-5}$. Thus, the minimum CIDS signal that we should expect our instrument to detect is about 7 parts in 10^5. In actual experiments, we found our typical limiting sensitivity to be in the range of 5×10^{-5} to 10^{-4}, in agreement with the above analysis.